

INVESTIGATION OF OPTOELECTRONIC PROPERTIES OF
BENZOTRIAZOLE AND THIAZOLE BEARING CONJUGATED POLYMERS

A THESIS SUBMITTED TO
THE GRADUATE SCHOOL OF NATURAL AND APPLIED SCIENCES
OF
MIDDLE EAST TECHNICAL UNIVERSITY

BY

HAKAN ÜNAY

IN PARTIAL FULFILLMENT OF THE REQUIREMENTS
FOR
THE DEGREE OF MASTER OF SCIENCE
IN
POLYMER SCIENCE AND TECHNOLOGY

JUNE 2019

Approval of the thesis:

**INVESTIGATION OF OPTOELECTRONIC PROPERTIES OF
BENZOTRIAZOLE AND THIAZOLE BEARING CONJUGATED
POLYMERS**

submitted by **HAKAN ÜNAY** in partial fulfillment of the requirements for the degree of **Master of Science in Polymer Science and Technology Department, Middle East Technical University** by,

Prof. Dr. Halil Kalıpçılar
Dean, Graduate School of **Natural and Applied Sciences**

Prof. Dr. Necati Özkan
Head of Department, **Polymer Science and Technology**

Prof. Dr. Ali Çırpan
Supervisor, **Polymer Science and Technology, METU**

Prof. Dr. Yasemin Arslan Udum
Co-Supervisor, **Technical Sciences Vocational School, Gazi University**

Examining Committee Members:

Prof. Dr. Levent Toppare
Chemistry, METU

Prof. Dr. Ali Çırpan
Polymer Science and Technology, METU

Prof. Dr. Yasemin Arslan Udum
Technical Sciences Vocational School, Gazi University

Assoc. Prof. Dr. İrem Erel Göktepe
Chemistry, METU

Assoc. Prof. Dr. Görkem Günbaş
Chemistry, METU

Date: 18.06.2019

I hereby declare that all information in this document has been obtained and presented in accordance with academic rules and ethical conduct. I also declare that, as required by these rules and conduct, I have fully cited and referenced all material and results that are not original to this work.

Name, Surname: Hakan Ünay

Signature:

ABSTRACT

INVESTIGATION OF OPTOELECTRONIC PROPERTIES OF BENZOTRIAZOLE AND THIAZOLE BEARING CONJUGATED POLYMERS

Ünay, Hakan

Master of Science, Polymer Science and Technology

Supervisor: Prof. Dr. Ali Çırpan

Co-Supervisor: Prof. Dr. Yasemin Arslan Udum

June 2019, 70 pages

This thesis deals with the design, synthesis and characterization of conjugated polymers **P1** and **P2** that have potential application in organic solar cell. Polymer design was accomplished by using band gap engineering method. According to that, benzodithiophene (BDT) and silafluorene were chosen as donor groups in **P1** and **P2** respectively. The acceptor parts were the same for both polymers including benzotriazole (BTZ) and thiazole group. According to electrochemical studies both polymers were having n-dopable and p-dopable characters. Highest occupied molecular orbital (HOMO) and lowest unoccupied molecular orbital (LUMO) levels of **P1** were determined as -5.63 eV and -3.60 eV, while **P2** had HOMO and LUMO energy levels -6.00 eV and -3.58 eV respectively. Optical band gap of **P1** and **P2** were calculated as 2.10 eV and 1.74 eV accordingly. Device construction was carried out with Bulk Heterojunction method and PCBM was used as the acceptor due to its suitable acceptor properties in polymeric solar cell applications. The best PCE was obtained from the device containing **P1**/PCBM 1:4 (w/w) ratio as 0.45 % under standard AM 1.5 G at 100 mW/cm².

Keywords: Benzodithiophene, silafluorene, thiazole, benzotriazole, conjugated polymers, organic solar cell

ÖZ

BENZOTRIAZOL VE TİYAZOL İÇEREN KONJUGE POLİMERLERİN OPTOELEKTRONİK ÖZELLİKLERİNİN İNCELENMESİ

Ünay, Hakan
Yüksek Lisans, Polimer Bilim ve Teknolojisi
Tez Danışmanı: Prof. Dr. Ali Çırpan
Ortak Tez Danışmanı: Prof. Dr. Yasemin Arslan Udum

Haziran 2019, 70 sayfa

Bu tez güneş pili alanında uygulama potansiyelleri bulunan konjuge polimerler olan **P1** ve **P2** polimerlerinin sentezi, tasarımı ve karakterizasyon çalışmalarını ele almaktadır. Polimer dizaynları bant aralığı mühendisliği metodu kullanılarak yapılmıştır. Bu bağlamda benzoditiyofen (BDT) ve silafuloren donör grupları olarak **P1** ve **P2** için seçilmiştir. Benzotriazol (BTZ) ve tiyazol grupları her iki polimer için de akseptör olarak kullanılmıştır. Elektrokimyasal çalışmalara göre her iki polimer de n-katkılanabilir ve p-katkılanabilir karakterler göstermiştir. En yüksek dolu moleküler orbital (HOMO) ve en düşük boş moleküler orbital (LUMO) seviyeleri **P1** polimeri için -5.63 eV ve -3.60 eV iken **P2** polimeri için ise HOMO ve LUMO değerleri -6.00 eV ve -3.58 eV olarak belirlenmiştir. **P1** ve **P2** polimerlerinin optik bant aralıkları sırasıyla 2.10 eV ve 1.74 eV olarak hesaplanmıştır. Cihaz yapımında yığımsal farklı türden eklemler metodu kullanılmış ve polimerik güneş pili uygulamalarındaki veriminden dolayı PCBM akseptör ünitesi olarak seçilmiştir. 1.5 G Hava Kütlesi (AM) ve 100 mW/cm² altında en yüksek güç dönüşüm verimi (PCE) değeri **P1**/PCBM 1:4 (w/w) oranında % 0.45 olarak gözlemlenmiştir.

Anahtar Kelimeler: Benzodityofen, silafuloren, tiyazole, benzotiriazol, konjüge polimerler, organik güneş pili.

To my family

ACKNOWLEDGEMENTS

Firstly I would like to thank Prof. Dr. Ali ırpan for his limitless patience during my long master period. It will be a honor for me to be his graduate student.

I am grateful to Prof. Dr. Levent Toppare, Assoc. Prof. Dr. Grkem Gnbař and Prof. Dr. Yasemin Arslan Udum for accepting to evaluate my thesis and their precious advice.

I owe special thanks to Soner ztrk for his unforgettable scientific support. It would be difficult for me to complete this thesis without him.

I would like to thank řevki Can Cevher and Kardelen Gksu for their help in thesis writing step.

I need to express my endless appreciation to Emre Ataođlu, Janset Turan and M. Genay elik for their friendship and support.

Thanks to all Cirpan and Toppare Research Group members for their cooperation.

I would like to express my deepest gratitude to my sister Hande nay for being the incentive that made me begin a journey in science.

I would like to express my gratitude to my parents for their effort on my life.

At the end, I would like to thank my life and my wife Gizem nay. Her love and devotion have beautified my world and this will continue forever.

TABLE OF CONTENTS

ABSTRACT	v
ÖZ	vii
ACKNOWLEDGEMENTS	x
TABLE OF CONTENTS	xi
LIST OF TABLES	xiv
LIST OF FIGURES	xv
LIST OF ABBREVIATIONS	xviii
1. INTRODUCTION	1
1.1. Solar Energy	1
1.2. Solar Energy Conversion into Electricity	1
1.2.1. A Brief History	1
1.2.2. Photoelectric Effect.....	2
1.2.3. Photovoltaic effect	2
1.2.3.1. Photovoltaics	3
1.3. Solar Cells	3
1.3.1. Efficiency of Solar Cells and Shockley and Queisser Limit	3
1.3.2. Methods for Exceeding SQ limit	4
1.3.2.1. Multijunction Solar Cells	5
1.3.2.2. Quantum Dots	6
1.3.2.3. Singlet Fission.....	7
1.4. Classification Solar Cells	7
1.4.1. Inorganic Solar Cells	8

1.4.2. Organic Solar Cells	10
1.4.2.1. Properties of Organic Molecules Used in Organic Solar Cells	11
1.4.2.2. Working Principle of Organic Solar Cells.....	11
1.4.2.3. Essential Parameters for Power Conversion Efficiency of Organic Solar Cells.....	14
1.4.2.4. Molecular Engineering for OPV.....	16
1.4.2.4.1. Design of Acceptor Materials	18
1.4.2.4.2. Design of Device and Interfacial Layer	19
1.5. Proof of Concept: Literature Review	20
1.6. Aim of This Study.....	25
2. EXPERIMENTAL	27
2.1. Materials and Equipments.....	27
2.2. Synthesis of Monomer	28
2.2.1. Synthesis of 4,7-dibromobenzo[c][1,2,5]thiadiazole (1).....	28
2.2.2. Synthesis of 3,6-dibromobenzene-1,2-diamine (2)	29
2.2.3. Synthesis of 4,7-dibromo-2H-benzo[d][1,2,3]triazole (3)	29
2.2.4. Synthesis of 9-(bromomethyl)nonadecane (4)	30
2.2.5. Synthesis of 4,7-dibromo-2-(2-octyldodecyl)-2H-benzo[d][1,2,3]triazole (5)	31
2.2.6. Synthesis of 2,2'-(2-(2-octyldodecyl)-2H-benzo[d][1,2,3]triazole-4,7-diyl)dithiazole (6).....	31
2.2.7. Synthesis of 2,2'-(2-(2-octyldodecyl)-2H-benzo[d][1,2,3]triazole-4,7-diyl)bis(5-bromothiazole) (M1) (7).....	33
2.3. Synthesis of Polymers.....	34
2.3.1. Synthesis of P1 (8)	34

2.3.2. Synthesis of P2 (9).....	35
3. RESULTS & DISCUSSION	37
3.1. Electrochemical Studies	37
3.2. Spectroelectrochemical Properties	40
3.3. Kinetic Studies	42
3.4. Thermal Analysis	44
3.5. Photovoltaic Studies	44
3.6. Optical Studies	47
4. CONCLUSIONS	49
REFERENCES.....	51
APPENDICES	57
NMR DATA	57
THERMAL ANALYSIS RESULTS	69

LIST OF TABLES

TABLES

Table 1. Electrochemical studies of polymer	39
Table 2. Summary of the spectroelectrochemical studies	41
Table 3. Optical Contrast and Switching Times of P1 and P2	43
Table 4. Photovoltaic studies based on P1 and P2	45

LIST OF FIGURES

FIGURES

Figure 1. Schematic Representation of Photoelectric Effect	2
Figure 2. The losses graph in an ideal silicon cell leading to the SQ limit. ¹²	4
Figure 3. Schematic representation for multijunction solar cell	6
Figure 4. Classification of Solar Cells	8
Figure 5. Schematic Representation of Solar Cell	9
Figure 6. Working Principle of Organic Solar Cells	12
Figure 7. Bulk Heterojunction.....	13
Figure 8. General design of an organic solar cell with bulk heterojunction	14
Figure 9. Hybridization of energy levels	16
Figure 10. Typical Conjugated Polymer	17
Figure 11. Representation of Internal Charge Transfer via Push – Pull Mechanism.	18
Figure 12. Chemical Structures of Fullerene Derivatives	19
Figure 13 Inverted and Conventional Solar Cells	20
Figure 14. Chemical Structure of benzo[1,2-b:4,5-b ₁] dithiophene.....	20
Figure 15. Chemical Structure of [3,4-b] thiophene(TT) and benzo[2,3,1] thiodiazole (BT)	21
Figure 16. Structures of PBDTTT, PbnDT-DTBT and F-PbnDT-DTBT.....	22
Figure 17. Inverted Solar Cell.....	23
Figure 18. Ternary Solar Cell Containing Non Fullerene Acceptor (Coi8dfic) and PTB7-Th and PC71BM.....	24
Figure 19. Structures of (COi8DFIC) and PTB7-Th and PC71BM.....	24
Figure 20. Chemical Structure of P1	25
Figure 21. Chemical Structure of P2	26
Figure 22. Retrosynthesis of M1	28
Figure 23. Synthesis of 4,7-dibromobenzo[c][1,2,5]thiadiazole.....	28

Figure 24. Synthesis of 3,6-dibromobenzene-1,2-diamine.....	29
Figure 25. Synthesis of 4,7-dibromo-2H-benzo[d][1,2,3]triazole.....	29
Figure 26. Synthesis of 9-(bromomethyl)nonadecane.....	30
Figure 27. Synthesis of 4,7-dibromo-2-(2-octyldodecyl)-2H-benzo[d][1,2,3]triazole	31
Figure 28. Synthesis of 2,2'-(2-(2-octyldodecyl)-2H-benzo[d][1,2,3]triazole-4,7- diyl)dithiazole.....	32
Figure 29. Synthesis of 2,2'-(2-(2-octyldodecyl)-2H-benzo[d][1,2,3]triazole-4,7- diyl)bis(5-bromothiazole).....	33
Figure 30. Synthetic Pathway for P1	34
Figure 31. Synthetic Pathway for P2	35
Figure 32. Cyclic Voltammogram of P1 at a scan rate of 100 mV/s.....	38
Figure 33. Cyclic Voltammogram of P2 at a scan rate of 100 mV/s.....	38
Figure 34. Electronic absorption spectra of the P1 in UV-Vis-NIR regions.....	41
Figure 35. Electronic absorption spectra of the P2 in UV-Vis-NIR regions.....	42
Figure 36. Percent Transmittance change for P1 at 500, 765 and 1315 nm.....	43
Figure 37. Percent Transmittance change for P2 at 490nm.....	44
Figure 38. I-V characteristics of photovoltaic devices based on P1 :PCBM(1:4), P1 :PCBM(1:3), P1 :PCBM(1:2), P1 :PCBM(1:1) blends.....	46
Figure 39. I-V characteristics of photovoltaic devices based on P2 :PCBM(1:3), P2 :PCBM(1:2) blends.	47
Figure 40. Absorbance spectra of P1	48
Figure 41. Absorbance spectra of P2	48
Figure 42. ¹ H NMR result of 9-(bromomethyl)nonadecane.....	57
Figure 43. ¹³ C NMR result of 9-(bromomethyl)nonadecane.....	58
Figure 44. ¹ H NMR result of 4,7-dibromobenzo[c][1,2,5]thiadiazole.....	59
Figure 45. ¹³ C NMR result of 4,7-dibromobenzo[c][1,2,5]thiadiazole.....	60
Figure 46. ¹ H NMR of 3,6-dibromobenzene-1,2-diamine.....	61
Figure 47. ¹³ C NMR of 3,6-dibromobenzene-1,2-diamine.....	62

Figure 48. ¹ H NMR of 4,7-dibromo-2-(2-octyldodecyl)-2H-benzo[d][1,2,3]triazole	63
Figure 49. ¹³ C NMR of 4,7-dibromo-2-(2-octyldodecyl)-2H-benzo[d][1,2,3]triazole	64
Figure 50. ¹ H NMR of 2,2'-(2-(2-octyldodecyl)-2H-benzo[d][1,2,3]triazole-4,7- diyl)dithiazole	65
Figure 51. ¹ H NMR of 2,2'-(2-(2-octyldodecyl)-2H-benzo[d][1,2,3]triazole-4,7- diyl)bis(5-bromothiazole)	66
Figure 52. ¹ H NMR of P1	67
Figure 53. ¹ H NMR of P2	68
Figure 54. TGA and DSC result of P1	69
Figure 55. TGA and DSC result of P2	70

LIST OF ABBREVIATIONS

EC	Electrochromic
CE	Coloration efficiency
LED	Light emitting diode
OLED	Organic light emitting diode
HOMO	Highest occupied molecular orbital
LUMO	Lowest unoccupied molecular orbital
OFET	Organic field effect transistor
PCE	Power conversion efficiency
CB	Conduction band
VB	Valence band
DA	Donor-Acceptor
OPV	Organic Photovoltaic
PET	Polyethylene terephthalate
ITO	Indium tin oxide
PSS	Polystyrenesulfonate
PEDOT	Polyethylene dioxythiophene
PCBM	[6,6]-Phenyl C 71 butyric acid methyl ester
BHJ	Bulk heterojunction
HIL	Hole injection layer

ETL	Electron transport layer
η	Power conversion efficiency
J_{sc}	Short circuit current density
V_{oc}	Open circuit voltage
FF	Fill factor
P_{max}	Maximum power
P_{in}	Power of the incident light
R_{sh}	Shunt resistor
R_s	Series resistor
AM 1.5G	Air mass 1.5 global
CV	Cyclic voltammetry
THF	Tetrahydrofuran
TBAPF6	Tetrabutylammonium hexafluorophosphate
ACN	Acetonitrile
NHE	Normal hydrogen electrode
E_g^{op}	Optic band gap
E_g^{el}	Electronic band gap
TGA	Thermal gravimetric analysis
DSC	Differential scanning calorimetry
UV	Ultraviolet
Vis	Visible
NIR	Near infrared

ICT	Intermolecular charge transfer
IPCE	Incident power conversion efficiency
EQE	External quantum efficiency

CHAPTER 1

INTRODUCTION

1.1. Solar Energy

Global warming will be the strongest issue on human life in the future. Its devastating results are increasing as folded. Even if it is an irreversible issue, in order to prevent its growing results on food supply, climate changes, and ecological balance, alternative energy sources are being researched. Depending on elevated fossil fuel consumption, CO₂ emissions have reached to dangerous limits. Enhanced global awareness has led to studies on green technologies. The most important among these is solar energy. With this respect, solar energy is not only crucial to make life possible in the world, but also it is essential to fulfill almost all type of energy demand of human being. It can be converted to other forms of energy such as fuel, heat, and electricity. The sun supplies enormous amount of energy to Earth, which is enough to satisfy all energy requirement of the world. The energy that is consumed by people annually is about 4.6×10^{20} J, reached Earth from the sun in one hour. With this information in hand, conversion of solar energy into electricity has become a fundamental research area over the past decades¹

1.2. Solar Energy Conversion into Electricity

1.2.1. A Brief History

Studies based on the conversion of solar energy to the electricity started in 1839 with the discovery of the "photoelectric effect", first perceived by a French physicist, Edmund Becquerel. He found that when light interacts with certain materials, it provides the formation of electricity²

In 1905, Albert Einstein published a landmark paper that is describing the nature of light and advancing the photoelectric effect with experimental data. According to this study, energy is thought as discrete quantized packages of energy, which is called as "photons"^{3,4} He won a Nobel Prize for his leading discovery.

1.2.2. Photoelectric Effect

Photoelectric effect is simply described as the electron emission from the exterior part of material after it expose to light. Each photon in a light beam has a certain energy that is proportional to its frequency. If an electron in a material absorbs a photon having lower energy than the binding energy of the material, it is ejected from the surface. If the photon possess less energy compared to the binding energy of the material, electron cannot escape from the material^{5,6}.

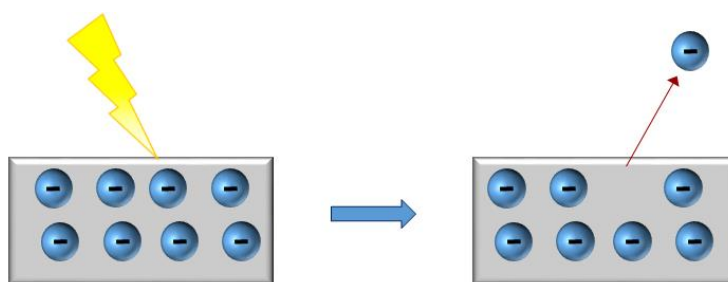


Figure 1. Schematic Representation of Photoelectric Effect

1.2.3. Photovoltaic effect

Discovery of photoelectric effect opened the gates of new research areas. In this manner, firstly photovoltaic effect was discovered. It is the formation of a voltage and electrical current when a material absorbs light. The difference between the photoelectric and the photovoltaic effect can be explained as follows: The former one is used when the electron is ejected while the latter one used when the excited electron is still on the material⁷.

1.2.3.1. Photovoltaics

These phenomena mentioned above gave rise to the invention of devices called as ‘photovoltaics’. As a general definition, photovoltaics are devices or materials provide the conversion of light into electricity in the form of current and voltage.

1.3. Solar Cells

Harnessing solar energy in the form of electricity via photovoltaics was started with the development of solar cells at Bell laboratories in 1954)⁸. This technology is presented as ‘Solar Battery’ at that time, and based on a silicon semiconductor and p-n junction.

1.3.1. Efficiency of Solar Cells and Shockley and Queisser Limit

Efficiency is defined as the ratio of energy converted to electricity to energy coming from the sun. This term does not only depend on the intensity of incident sunlight, but also depends on the performance of solar cell. Since there are a lot number of parameters that affect the efficiency, it has a limit.

Calculation of the efficiency limit was firstly attempted by Shockley and Queisser in 1961⁹. Calculation based on the determination of the quantity of energy in terms of electricity obtained from photon. The maximum theoretical efficiency of solar cells is known as Shockley-Queisser (SQ) Limit and it is approximately 33.16% for a single junction cell. In this calculation, typical sunlight conditions was used as a base (unconcentrated AM 1.5 spectrum of the Sun and takes place at a bandgap of 1.34 eV)¹⁰. That means of input and output power is W/cm^2 , the conversion efficiency is named as Power Conversion Efficiency (PCE) and of all the power of sunlight coming to an ideal solar cell, 33,16% of that incident power could be turned to electricity⁹. The most well-known solar cell material, silicon, has a band gap at around 1.1 eV and it causes the decrease in the maximum efficiency which is at 32%¹⁰.

The loss of efficiency can be explained with a general mechanism called as thermalization. According to this mechanism, photons having an energy above the band gap energy is ruined in the form of heat. Besides the thermalization, the main reason of Shockley-Queisser limit is non absorbed photons that have less energy than the band gap energy¹¹.

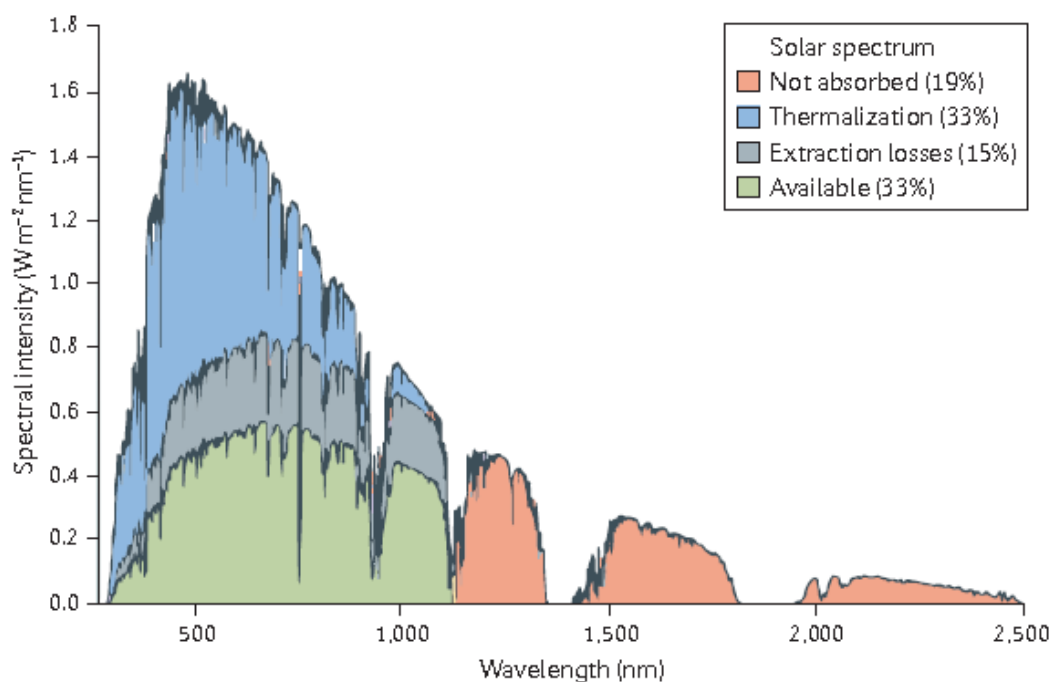


Figure 2. The losses graph in an ideal silicon cell leading to the SQ limit.¹²

Since gathering the full spectrum of sun is not possible due to Shockley-Queisser limit, it has become a problem for conventional single junction photovoltaics. In order to exceed SQ limit scientists have searched new technologies over 50 years.

1.3.2. Methods for Exceeding SQ limit

In order to achieve better efficiency with exceeding SQ limit some basic strategies listed below are applied¹³⁻¹⁵.

- ✓ Use of more than one semiconductor material in a cell
- ✓ Use of more than one junction in a cell. These types of cells are called as ‘tandem cells’.
- ✓ Use of inexpensive lenses in order to concentrate sunlight about 500 times.
- ✓ Combination of a photovoltaic semiconductor devices with a heat based technology. Thus one can collect both forms of energy.
- ✓ Use of multiple exciton generation that are quantum dots and singlet fission.

Among them the most striking methods are use of multijunction solar cells and use of multiple exciton generation.

1.3.2.1. Multijunction Solar Cells

As it can be understood from the name, multijunction solar cells consist of multiple connection with different semiconductor materials that come together to broaden absorbed spectrum of the sunlight. Layers containing different materials are placed successively and band gap of the materials decrease from top to bottom of device. According to theoretical calculations, use of infinite number of p-n junctions, would increase the efficiency up to 86% under concentrated sunlight¹⁵. Although generation of multijunction solar cell raises the efficiency up to 45% it does not satisfy the expectations due to high cost and advanced engineering requirements.

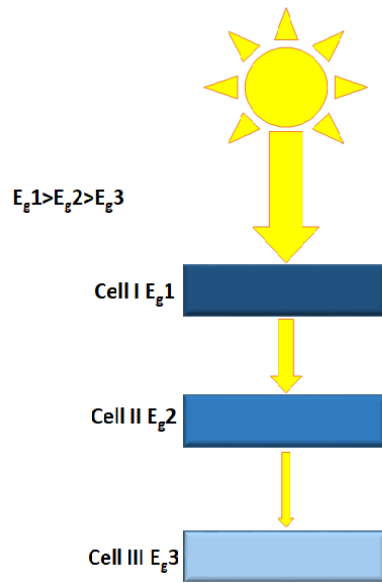


Figure 3. Schematic representation for multijunction solar cell

1.3.2.2. Quantum Dots

The second approach is the utilization of multiple exciton generation (MEG, also termed as carrier multiplication). Unlike the conventional solar cell working principle, excited carriers can donate some of their energy to another electron resides in ground state. By this way this electron can also pass the band gap of corresponding semiconductor. It means that single photon has a potential to create multiple electron hole pair by using MEG method¹⁶ In quantum dots (QD), quantum wires (QW) and quantum rods (QR) this process is applicable, since they have properties between conducting and semiconducting materials. Like conductors QD, QW and QR's that are made from same material have quantized energy levels, but depending on the sizes of them, they emit light at different wavelengths. Larger quantum dots emits longer wavelengths which have colors from red to orange, while smaller ones emits shorter wavelengths and they have colors from green to blue. The reason of this phenomena is explained with the band gap difference. Small dots have bigger band gaps, they need more energy to excite electron found at ground state. Small dots having higher energy

generate higher frequencies and shorter wavelengths. On the other hand larger dots have more closer band gap, hence they emit at lower frequencies and higher wavelengths¹⁴⁻¹⁷

In order to obtain exciton multiplication, the absorbed photon must have at least twice of the band gap energy. Although multiple exciton generation provides new field for the generation of solar cell, the efficiency of this process is not sufficient enough¹⁸.

1.3.2.3. Singlet Fission

The last method that overcoming thermalization problem is called as Singlet Fission. Singlet fission is also a kind of carrier multiplication process that is obtained from semiconductor. From this point of view SF and QD has common ground that is multiple exciton generation. The main difference is, in QD method, inorganic compounds are used but for SF process organic based materials have a leading role. Singlet fission is prevalent for molecular chromophores, those triplet energy state (T_1) is half of the first excited energy state (S_1). In that process excited chromophore molecule shares some of the energy with another neighboring ground state chromophore molecule. As a result, both of them are present at their triplet energy state^{19,20}

1.4. Classification Solar Cells

According to junction applications, solar cells are classified into three main category:

- Inorganic p-n junction–based solar cells
- Organic e-donor/e-acceptor junction–based solar cells
- Hybrid junction–based solar cells

The third group is further classified into two subgroup which are dye-sensitized solar cells and other hybrids. As an example for the other hybrid solar cells nanostructured inorganic solar cells and organic matrix solar calls can be shown²¹.

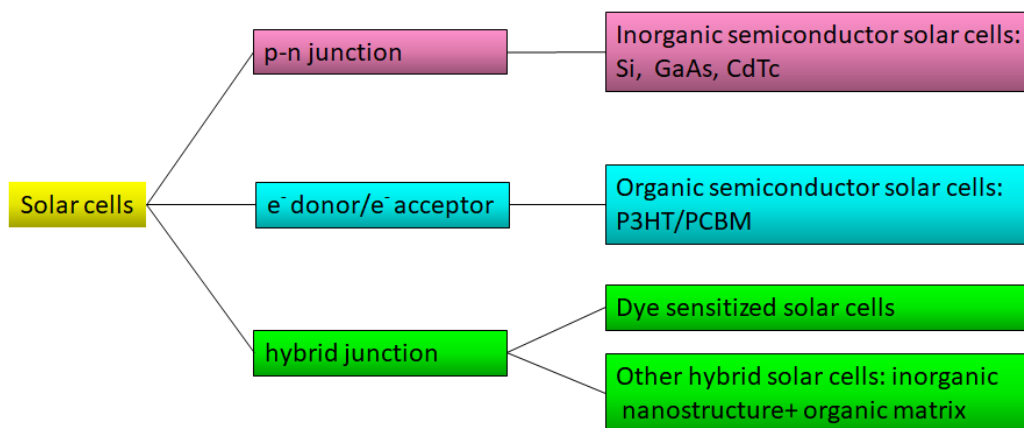


Figure 4. Classification of Solar Cells

1.4.1. Inorganic Solar Cells

p-n junction is a connection boundary between two types of semiconductors, p-type (excess hole) and n-type (excess electron). The discovery of p-n junction is associated with American physicist Russell Ohl in Bell Laboratories.

A typical solar cell consists of two semiconductors; n-type and p-type silicon. By adding atoms (boron or gallium) p-type silicon can be produced. Due to electron vacancy hole is created. n-type silicon is produced by adding atoms that have one more electron in their outer shell than silicon, like phosphorus. Thus one electron moves freely in silicon.

A layer of p-type silicon is placed on the layer of n-type silicon. n-type layer contains excess electrons, while p-type contains excess of positively charged holes. Electrons on the side of n-type layer move into the holes of p-type layer near the junction of two layers. This region is called as depletion zone. In here holes are filled with electrons.

When electrons fill the holes in depletion zone, p-type side of depletion zone which previously contains holes, now has negatively charged ions. On the other hand, n-type side of the zone where initially electrons exist now contains positively charged ions. Due to occupancy of oppositely charged ions, formation of internal electric field

prevents the movement of electrons in the n type layer through the holes in p-type layer.

Interaction with sunlight causes ejection of electrons from silicon and thereby holes are formed. Presence of internal electric field in solar cell leads to move electrons to n-type layer, and holes to p-type layer. If these layer are connected with a metallic wire electrons will go from n-type layer to p-type by passing the depletion zone and then travel through the external wire back of n-type layer. This situation generates flow of electricity²².

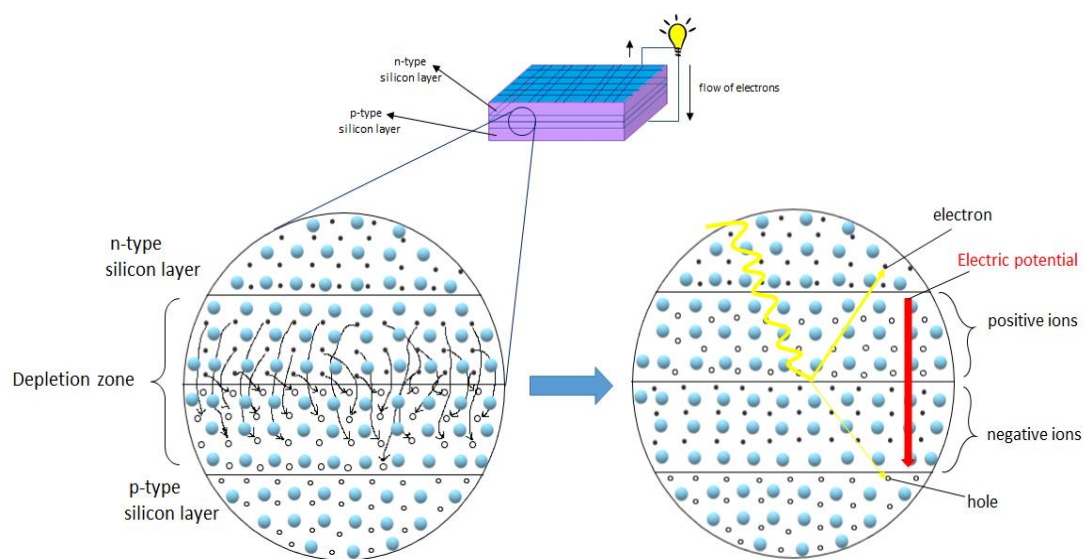


Figure 5. Schematic Representation of Solar Cell

Among the semiconductors, silicon (Si) is one of the most plentiful element in Earth crust. For about 90% of the photovoltaic applications crystalline form of silicon (c-Si) is utilized. Although other type of semiconductors give higher efficiency, silicon based solar cells dominates the worldwide scientific research area and industry. The main reason of it could be the low-cost, high-yield process, well characterized device properties and suitable band gap. Band gap for the silicon is 1.1 eV. This value is reasonable for solar cell applications since the ideal band gap should be about 1.3 eV for the maximum efficiency as mentioned in Efficiency of Solar Cells chapter. Other materials are in progress for commercialization or need further developments. Among

them, amorphous silicon (a-Si), cadmium telluride (CdTe) and copper indium gallium diselenide (Cu(InGa)Se₂ or CIGS) draw most attention.

To enhance the efficiency and reduce cost of solar cells optical components such as lenses and mirrors could require. Instead of illuminating larger area with the light, use of these components as concentrators provides minimization of solar cell area yet the insertion of them adds complexity to the system. In addition to these, utilization of compounds such as gallium arsenide (GaAs) and gallium indium phosphide (GaInP) as a semiconductor accompanied with silicon increases the efficiency. However these type of solar cells use only in spaceship applications for now²³.

1.4.2. Organic Solar Cells

Organic solar cell is a type of device that converts light into electricity using organic polymers or organic small molecules. These compounds belong to a special field called ‘‘organic electronics’’. Their synthesis, characterization, electronic properties (conductivity) and application have gain importance in recent years due to their superiority over inorganic analogue such as low cost, lightweight, flexibility, potential to exhibit transparency²⁴.

The history of organic solar cells has begun with the seeking of cheaper alternatives than semiconductor grade silicone organic dyes have drawn attraction as a potential for solar cell applications due to their strong optical absorption and regional absorption of solar spectrum. From this point of view, chlorophyll was used in photoelectrical devices in 1970 by Tang and Albrecht²⁵. Utilization of organic dyes in organic optoelectronic devices was continued at Kodak Research Lab by Tang and organic dyes were applied to the bilayer devices. A prototype of organic photovoltaic device was reported in 1986 by Tang with 1% power conversion efficiency (PCE) under sunlight²⁶.

1.4.2.1. Properties of Organic Molecules Used in Organic Solar Cells

With these promising results obtained from small organic molecules, polymers were also started to use in photovoltaic devices. Both small molecules and polymers have a common characteristic that they all have conjugation over whole molecule. For the formation of conjugated system, covalently bonded carbon atoms having alternating single and double bonds is crucial.

The electrons of these hydrocarbons are on p_z orbitals and produce two new orbital systems:

- delocalized bonding π orbital
- delocalized antibonding π^* orbital

In this case delocalized bonding π orbital is also called as the highest occupied molecular orbital (HOMO) and the latter one is called as the lowest unoccupied molecular orbital(LUMO). In organic solar cell system HOMO behaves as the valence band while LUMO takes the role of the conduction band. Bandgap between HOMO and LUMO in organic compounds is typically between 1-4 eV²⁷.

1.4.2.2. Working Principle of Organic Solar Cells

The main difference between the working principles of organic solar cell and the inorganic analogue is the organic photovoltaics are not in crystalline form. Since there are no bands for electrons and no electric field for the movement of electrons, excited electrons formed by the absorption of light, recombine with its hole as soon as it is created. To prevent this recombination, organic photovoltaics need two materials, one of them is for holes and the other one is for electrons²⁸

Under the light of these informations, essential steps of the photon to electron conversion mechanism in organic photovoltaics are illustrated in Figure 6.

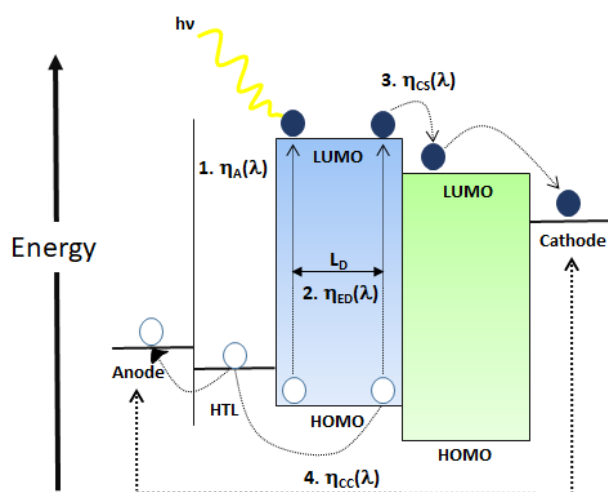


Figure 6. Working Principle of Organic Solar Cells

In the first step, absorption of light causes the excitation of the electron from HOMO to LUMO of the organic material with the formation of Frenkel exciton (figure 6). Frenkel exciton is a bound form of electron (e^-) and hole (h^+) with the help of coulombic forces. If the number of Frenkel excitons is divided by the number of incident photons, the resulting ratio gives the absorption efficiency (μ) in terms of energy.

To separate excitons into holes and electrons, electron acceptor material is required. By this, between the interface of the donor and acceptor material internal field is formed and excitons break up to holes and electrons. As a result, they can diffuse into free carriers. The most extensively used materials as an acceptor are fullerenes since they have higher electron affinities than those of polymers or small molecules used as donor²⁹.

In the second step, diffusion of exciton to the donor acceptor (D-A) interfaces is the key part of the process. To prevent recombination of e^- and h^+ diffusion length (L_D) is very crucial. To maximize the interface surface area to volume ratio, donor and acceptor materials are been mixed or been made very thin films of the material (donor

or acceptor) on top of the remaining one formed Bulk Heterojunction shown in Figure 7³⁰.

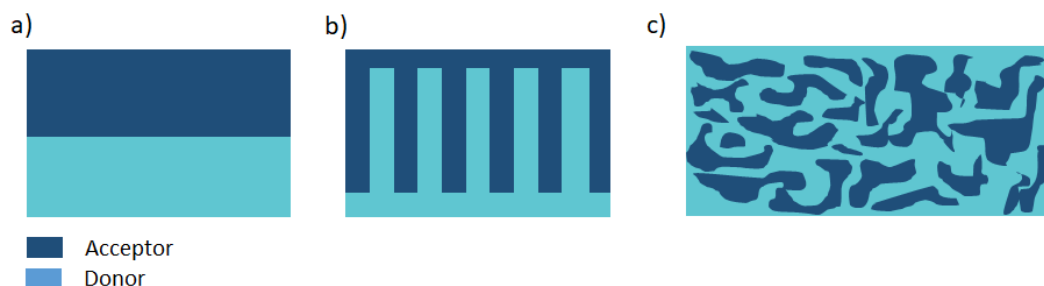


Figure 7. Bulk Heterojunction

The value of L_D for organic compounds is typically 10 nm^{31} . Furthermore, the optimum domain size must be smaller than 20 nm.

In terms of charge transportation donor-acceptor (D-A) interface concept is akin to a p-n junction in semiconductors consist of inorganic materials. Exciton diffusion efficiency (η_{ED}) can be calculated by dividing the amount of excitons that arrive to D-A junction to the number of excitons that formed after photo-excitation.

In the third step, excitons that arrived to D-A junction are subjected to charge transfer (CT) process. This process takes place in 100 fs ³² and in this process holes and electrons stay at donor and acceptor phases accordingly. Excitons that are formed in CT process called as CT exciton. The ratio between the quantity of excitons subjected to charge transfer process and the amount of excitons which arrive to D-A interface can be defined as the charge separation efficiency (η_{CS}).

In the fourth step, CT excitons separated as free holes and electrons due to deformation of the built-in electric field. These independent electrons and holes moved through the related donor and acceptor material accordingly and finally moved to related electrodes. Dividing the number of charge carriers, that reach to electrodes to the

quantity of excitons that are subjected to charge transfer process give the charge collection efficiency (η_{cc}).

Organic layers that are mentioned above are not the only necessary parts of the solar cells. Design of the components are also crucial for the working mechanism of the solar cells. Transparent conducting electrode is required on the side where incident light reach to the solar cell. Indium thin oxide (ITO) is a widely used material to afford this requirement. For the mechanical support, glass substrate is used. To minimize losses coming from non-absorption, anti-reflection coatings are necessary. Besides, to obtain dark sided electrode, thin film of the certain metals such as Al or Au has been utilized by evaporation on to the device. General design of an organic solar cell with bulk heterojunction is shown below. (Figure 8)⁷.

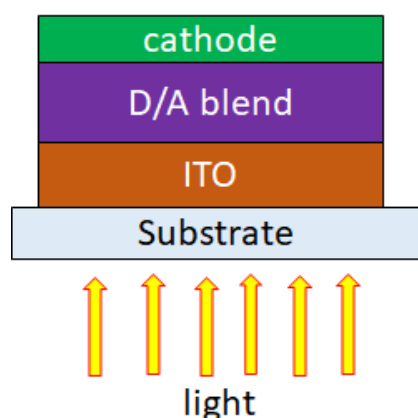


Figure 8. General design of an organic solar cell with bulk heterojunction

1.4.2.3. Essential Parameters for Power Conversion Efficiency of Organic Solar Cells

External quantum efficiency (EQE) is used for evaluation of OPV devices, it explains the ratio of generated charges to collected energy from photons.

EQE is one of the most important parameter for a conversion process from photon to electron. The EQE is defined by the equations shown below (1):

$$\text{EQE}(\lambda) = \eta_A(\lambda) \times \eta_{\text{ED}}(\lambda) \times \eta_{\text{CS}}(\lambda) \times \eta_{\text{CE}}(\lambda) \quad (1)$$

(λ) = wavelength of the incident light

Furthermore, power conversion efficiency (PCE, $\eta\%$) is expressed by the equation (2)

$$\eta = \frac{(\text{J}_{\text{sc}} \times V_{\text{oc}} \times \text{FF})}{P_{\text{in}}}$$

J_{sc} \longrightarrow short circuit current density

V_{oc} \longrightarrow open circuit voltage

FF \longrightarrow fill factor

P_{in} \longrightarrow power of incident light

Width of the absorbed spectrum of the light determines J_{sc} , which means it depends on band gap. Besides, it is regulated by the thickness and morphology of the active layer. Arrangement of active layer also influences FF value. Additionally V_{oc} can be defined as the maximum potential when there is no flow. Theoretically open circuit voltage is directly depends on the energy difference between the HOMO of the donor and LUMO of the acceptor. Increase in the value of V_{oc} means also increase in the value of power conversion efficiency (PCE) as seen in eq. (2). To enhance the value of V_{oc} , HOMO of the donor can be lowered or LUMO of the acceptor can be raised. In this approach, there is also an important criteria that is the LUMO of the donor must be higher at least 0.3 eV than the acceptor³³.

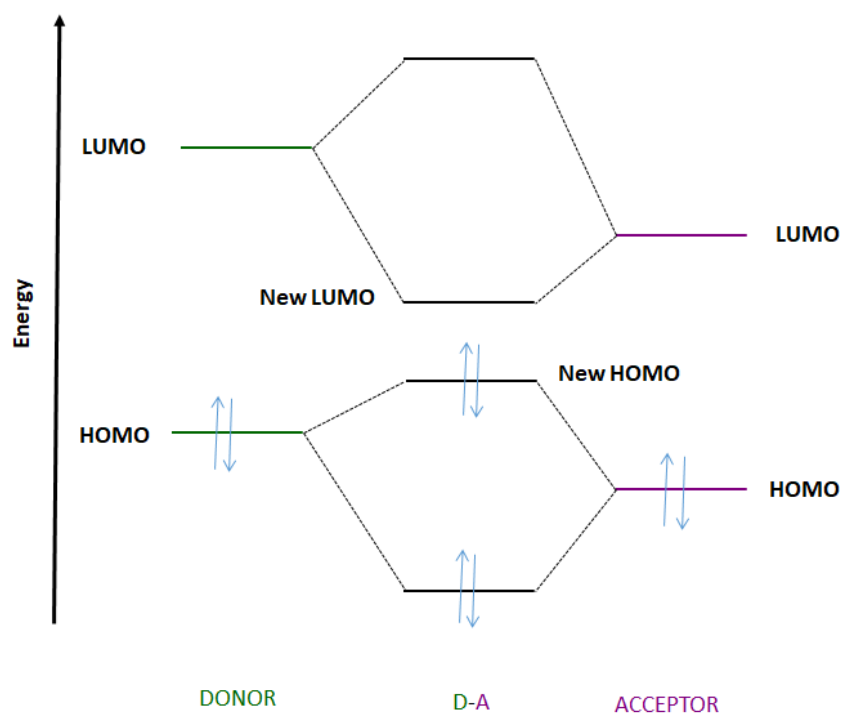


Figure 9. Hybridization of energy levels

1.4.2.4. Molecular Engineering for OPV

For the application in the field of organic photovoltaics, polymers or small molecules must have some basic properties listed below:

1. Low bandgaps; to widen the absorption region,
2. Crystalline characteristic; to provide proper charge mobility,
3. Low HOMO energy level; to increase the value of V_{oc}
4. Appropriate LUMO energy levels for the transfer of electrons through fullerene.

From this point of view, design of the conjugated polymers is based on three features of it (Figure 10)³⁴.

- Backbone repeating unit
- Substituents

- Side chains

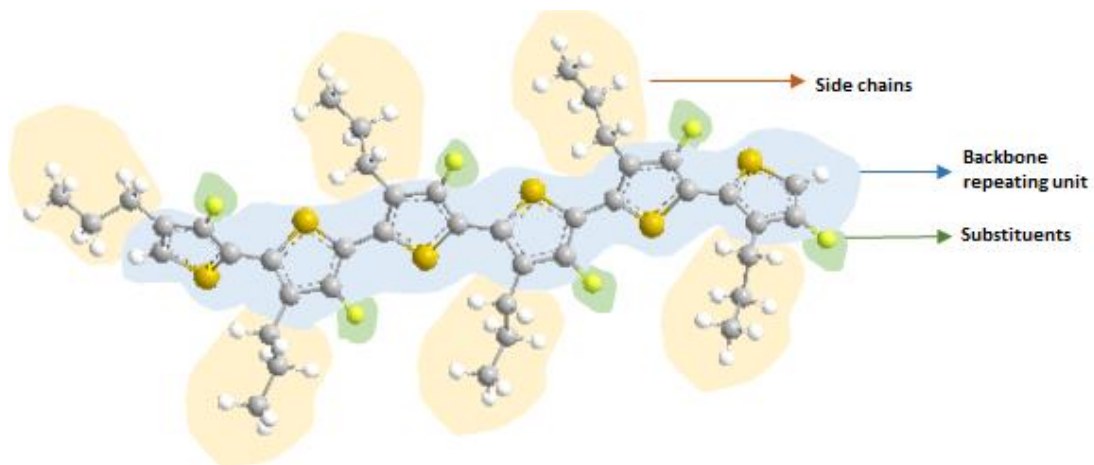


Figure 10. Typical Conjugated Polymer

HOMO and LUMO energy levels, as well as band gap are determined by the backbone repeating units having conjugated chains. When the molecular weight of the polymer is less than 10000 Da it must be under consideration during the determination of band gap.

Implementation of e^- push and pull molecular parts to the conjugated chain is the most effective method for gathering photons as much as possible.

Alternated push and pull units provides internal charge transfer through the conjugated main chain. The length of the resonance π electrons is enhanced by the same strategy. As a conclusion of that simplified πe^- delocalization smaller band gaps are observed³⁵.

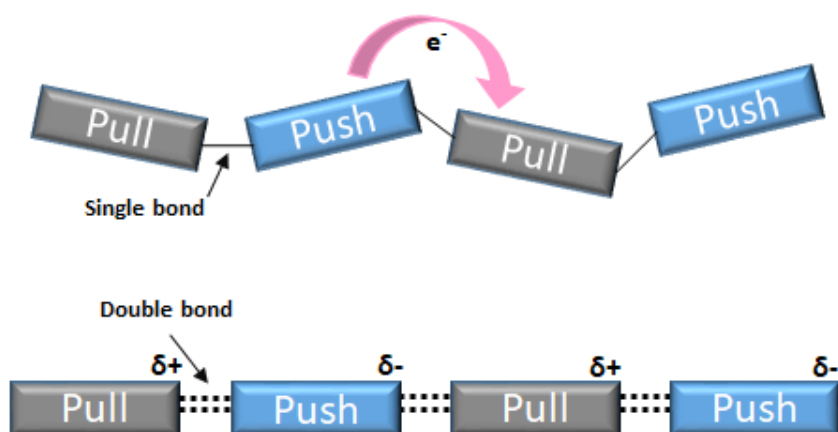


Figure 11. Representation of Internal Charge Transfer via Push – Pull Mechanism

Another important feature is the planarization. As it is mentioned above, HOMO and LUMO levels of conjugated polymer play an important role for enhanced PCE. Therefore, in order to reduce the energy level of HOMO and the bandgap of the corresponding polymer, weakly e^- donating group connected to a strongly e^- withdrawing one is crucial to satisfy these energy level requirements. By this way V_{oc} and J_{sc} can be increased simultaneously when polymer is blended with fullerenes³⁶.

1.4.2.4.1. Design of Acceptor Materials

Due to the strong electron affinity and good solubility, fullerene derivatives have been used as the acceptor materials in solar cell applications over decades. Mostly used fullerene derivatives, PC₆₁BM and PC₇₁BM, are also self-assembled into certain parts of the active layer. Figure 12 shows the chemical structures of these fullerene derivatives used as the acceptors.

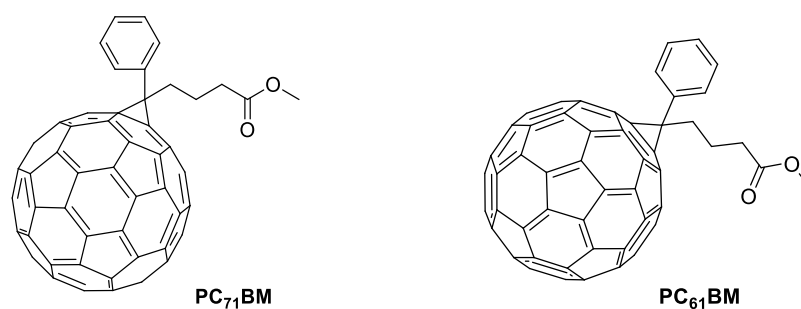


Figure 12. Chemical Structures of Fullerene Derivatives

1.4.2.4.2. Design of Device and Interfacial Layer

Stability of OPV is one of the main priority for the design process. Beside the stability, materials that can be used in OPV must also be processable. Under the light of these informations, two main device design, conventional and inverted, have been recently used in OPV devices. In these two design ITO-based electrode has two configurations: Glass/ ITO/ Polyethylene dioxythiophene:polystyrene sulfonate (PEDOT:PSS)/ active layer/ electron transport layer (Ca or LiF/Al) and low work function electrode (Al) configuration belongs to conventional device structure. PEDOT:PSS is used as the hole transport layer (HTL) and Ca or LiF/Al is used as the electrode transport layer (ETL). ITO is utilized as an anode while Al behaves as the cathode. Since low work function electrode is unstable in air, encapsulation of the electrode plays an important role for device stability. To solve air unstability problem inverted device design have been used currently. In this geometry glass/ITO/electron transport layer/active layer/hole transport layer and high work function electrode were used. This design gives high stability to device since high work function metal such as Ag and Au are introduced as the top electrode. The main issue of this design is the use of expensive metals as a cathode³⁷.

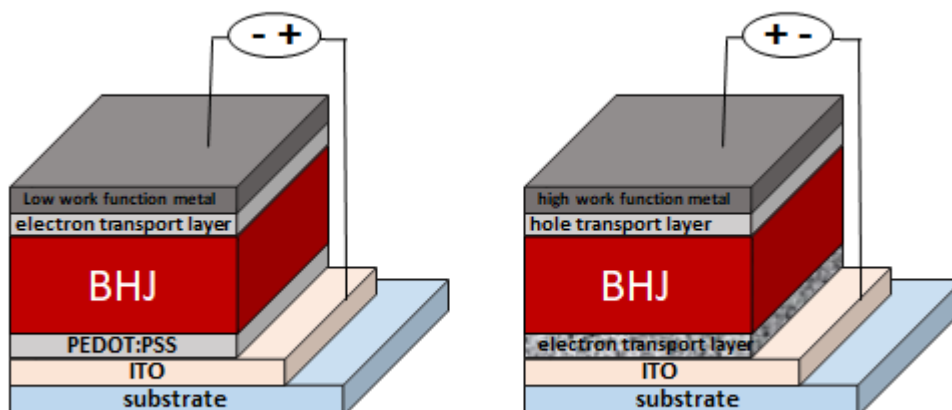


Figure 13 Inverted and Conventional Solar Cells

1.5. Proof of Concept: Literature Review

There are several conjugated polymers that are designed under the light of these informations³⁸⁻⁴³.

One of the most efficient units having planar structure and e^- push ability is benzo[1,2-b:4,5-b'] dithiophene. (BDT) Figure 14. Integration of BDT unit in a polymer containing e^- push and pull alternating structure as a push unit provides a low bandgap 1.8 eV and lower the HOMO energy level. By using it, PCE is obtained in photovoltaic devices between 5-7%^{44,45}.

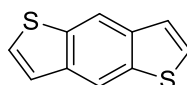


Figure 14. Chemical Structure of benzo[1,2-b:4,5-b'] dithiophene

Similarly, [3,4-b] thiophene(TT) and benzo[2,3,1] thiodiazole (BT) can be counted as the effective electron push units (Figure 15).

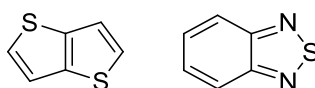
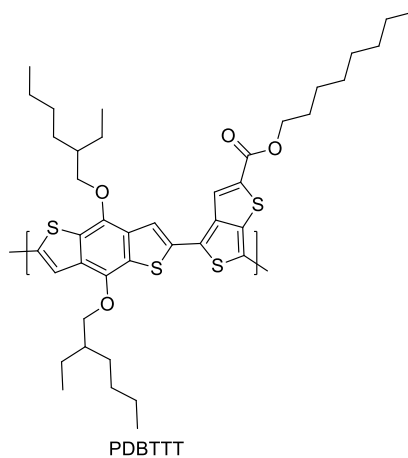


Figure 15. Chemical Structure of [3,4-*b*] thiophene(TT) and benzo[2,3,1] thiodiazole (BT)

To build conjugated planar polymer containing push and pull units, BDT were used as the push unit and TT and BT were incorporated to the polymers. As a result of polymerization of BDT with TT and BT, PBDTTT⁴⁶ and PbnDT-DTBT⁴⁷ were obtained respectively. Use of PC₇₁BM as an acceptor resulted in the obtaining PCE higher than 5%. As it is expected substitution of hydrogen atoms on thiophene ring in PBDTTT polymer and hydrogen atoms on phenyl ring in PbnDT-DTBT polymer with fluorine atoms causes decrease in both HOMO and LUMO's of corresponding polymer. As a result of it PCE reaches to a level higher than 7% (Figure 16).



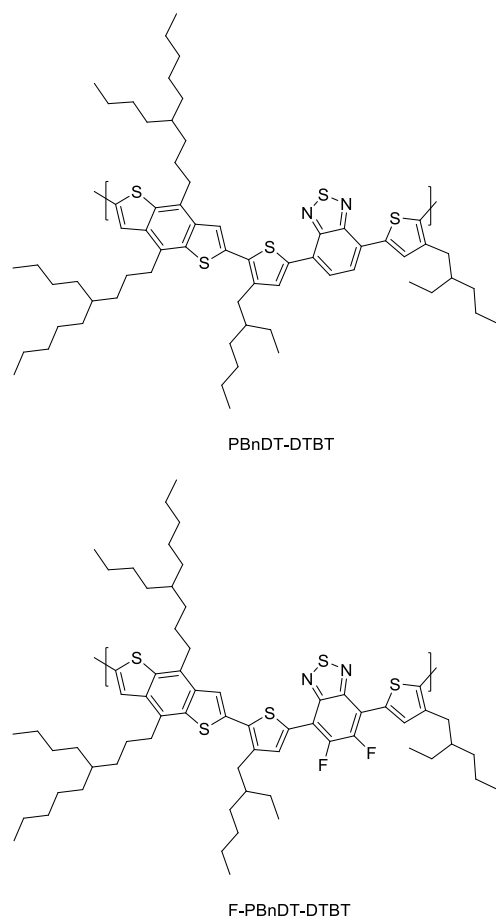


Figure 16. Structures of PBDTTT, PbnDT-DTBT and F-PbnDT-DTBT

In 2012 He *et al.* synthesized and characterized organic solar cells containing polymer fullerene solar cell with high efficiency (PSCs). Using an inverted structure and poly[(9,9-bis(3¹-N,N-dimethyl(amino)propyl)-2,7-fluorene)-alt-2,7-(9,9,-dioctylfluorene)] (PFN) as the ITO surface modifier, and a blend of PC₇₁BM and the low bandgap polymer thieno[3,4-b]thiophene/benzodithiophene (PTBZ) as the photoactive layer device design was completed Figure 17.

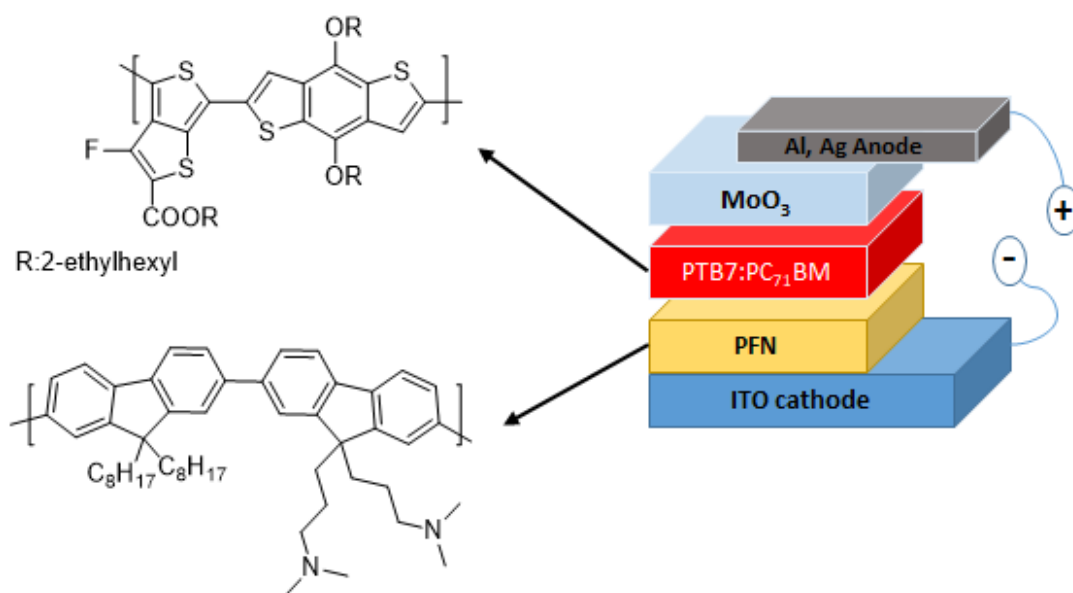


Figure 17. Inverted Solar Cell

As it is mentioned in the previous chapter in an inverted cell, the positive and negative electrodes are reversed and as a result of it electric charges leave the cell in opposite way. The efficiency of corresponding PSCs was reported as 9.2% by He et al. This promising result open up new occasions to increase the efficiency of PSC's up to 10%⁴⁸.

In 2018 Li et al designed ternary a solar cell containing non fullerene acceptor (CO₈DFIC) and PTB7-Th and PC₇₁BM (Figure 18). The efficiency of PCS's was found as 14.62% and the device showed satisfying thermal stability with PCE over 13.5% between 70-160 °C. As it is shown in Figure 18 alignment of energy levels provides electron transfer from PTB7-Th to CO₈DFIC via PC₇₁BM efficiently. For the commercialization of organic cells, use of CO₈DFIC gave promising results⁴⁹.

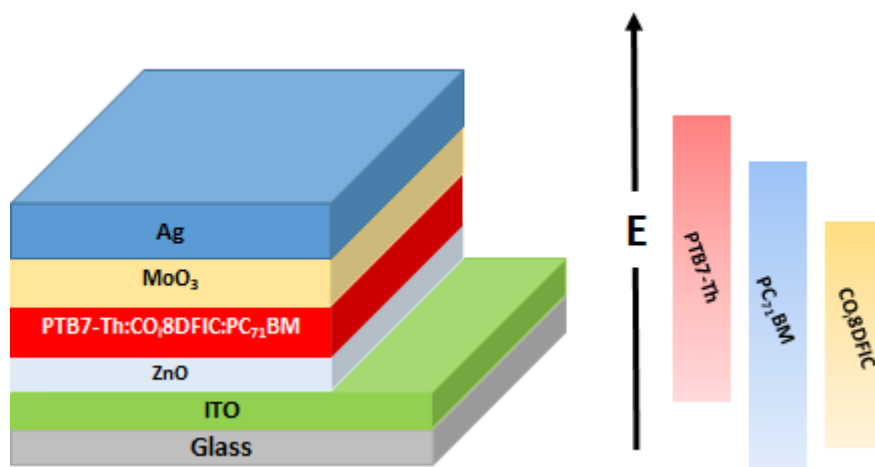


Figure 18. Ternary Solar Cell Containing Non Fullerene Acceptor (Coi8dfic) and PTB7-Th and PC71BM

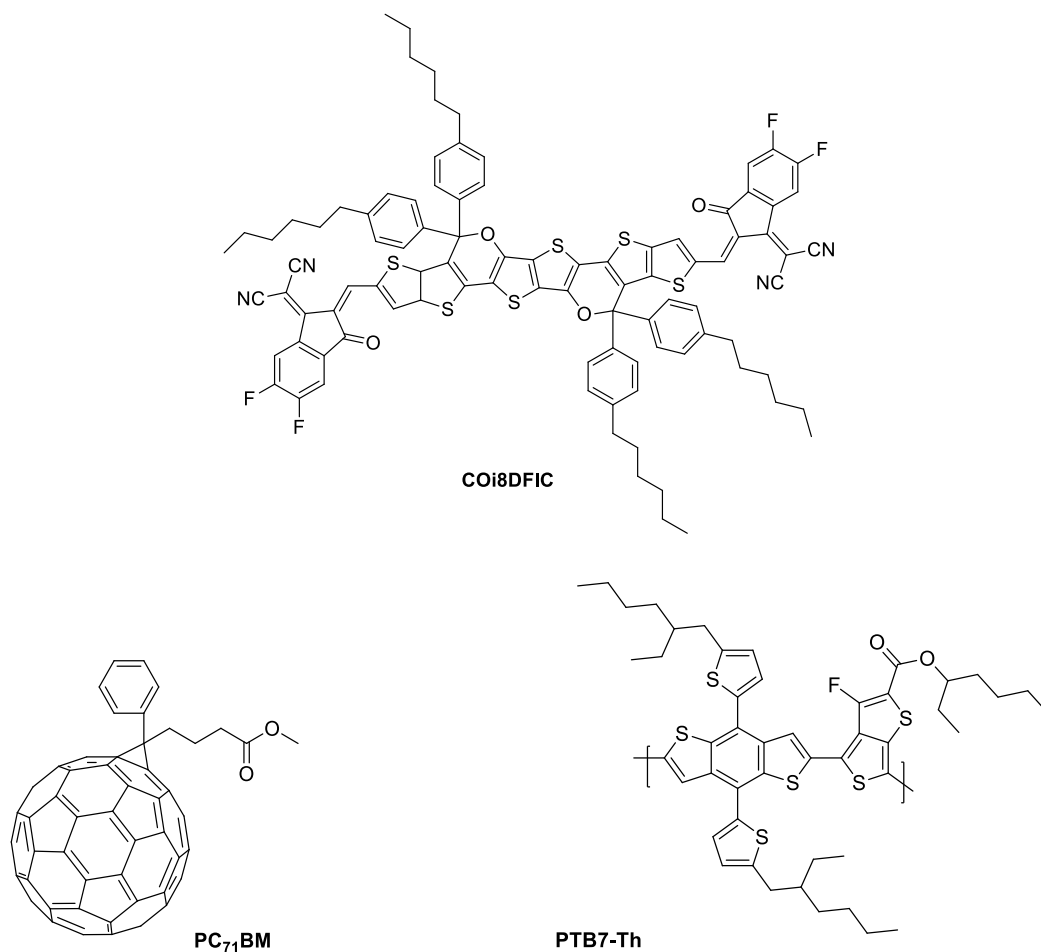


Figure 19. Structures of (Coi8DFIC) and PTB7-Th and PC71BM

1.6. Aim of This Study

The countless opportunities and application areas of conjugated polymers was outlined in the introduction part. Among them one of the most essential one is their potential applications in solar cell area, since conversion of the solar energy in to the electricity is crucial due to the descending non-renewable energy sources on earth. Under the light of this motivation, two polymers were designed to fulfill requirements for a solar cell. During the polymer design process, donor-acceptor approach was utilized to achieve low band gap polymers. For this, benzotriazole and thiazole moieties were chosen as the acceptor parts of polymers. As a donor part, two different compounds, BDT and silafluorene, were used. Stille and Suzuki coupling reactions were the key method for the synthesis of these polymers. After synthesis of the polymers, their optoelectronic properties were investigated.

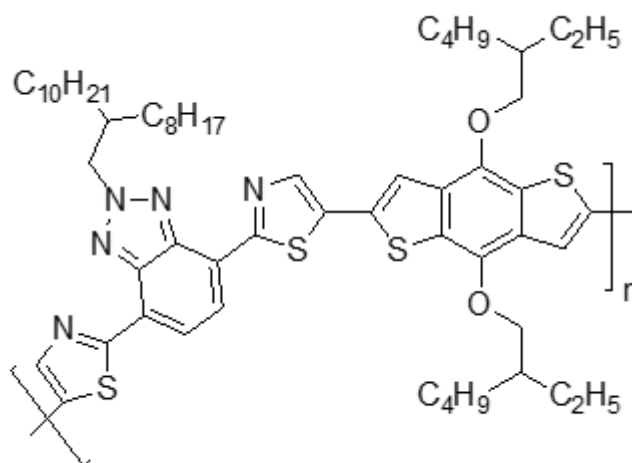


Figure 20. Chemical Structure of **PI**

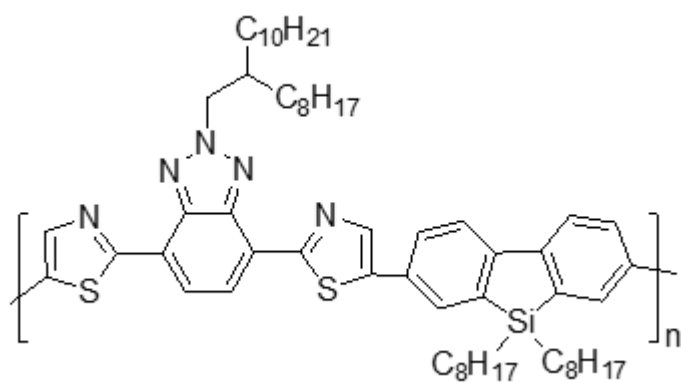


Figure 21. Chemical Structure of **P2**

CHAPTER 2

EXPERIMENTAL

2.1. Materials and Equipments

Reagents and solvents used in the synthesis of monomers and polymers were purchased from Sigma-Aldrich. PC₇₁BM, serves as the acceptor in solar cell device was purchased from Solanne. Toluene was dried with standard laboratory procedure that includes metallic sodium and benzophenone. All other solvents and reagents were used without further purification. Reactions that are sensitive to air and moisture was performed under Argon atmosphere.

For purification, column chromatography method was utilized and Merck Silica Gel 60 was chosen as the stationary phase. For the characterization of the monomers and polymers ¹H and ¹³C NMR spectra were used and measurements were performed with A Bruker Spectrospin Avance DPX-400 Spectrometer. Interpretation of chemical shifts were done relative to CDCl₃ at $\delta=7.24$ ppm and tetramethylsilane at $\delta =0.00$ ppm. To determine number and weight average molecular weight of polymers gel permeation chromatography (GPC) method was performed. Polystyrene was used as the reference and chloroform was used as the solvent. Gamry Reference 600 Potentiostat/Galvanostat and Varian Cary 5000 UV-Vis spectrophotometer were the instruments that were used to measure electrochemical, spectroelectrochemical and colorimetric results respectively.

2.2. Synthesis of Monomer

Retrosynthetic analysis of monomer **M1** is shown in scheme below:

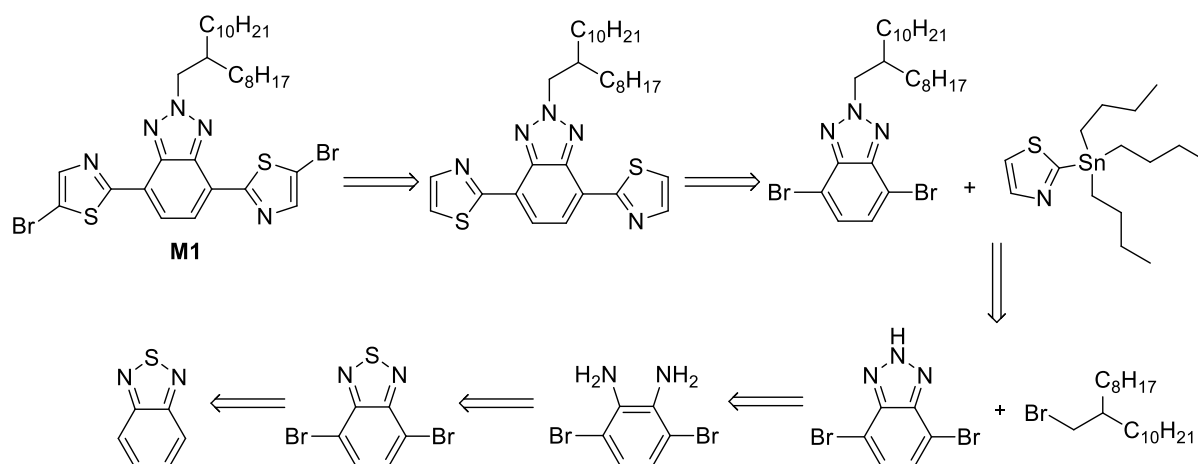


Figure 22. Retrosynthesis of **M1**

2.2.1. Synthesis of 4,7-dibromobenzo[*c*][1,2,5]thiadiazole (**1**)

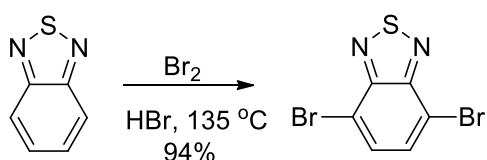


Figure 23. Synthesis of 4,7-dibromobenzo[*c*][1,2,5]thiadiazole

2,1,3-benzothiadiazole (5.00 g, 36.7 mmol) and 50 mL HBr (47%) were stirred and refluxed at 100 °C for one hour under Ar(g). To the mixture, bromine (5.50 mL, 108 mmol in HBr (20 mL, 47%) was added dropwise and refluxed overnight. Resulting mixture was poured into concentrated NaHSO₃ solution (600 ml) to remove excess Br₂. After filtration, orange precipitate was observed. Solids were washed with distilled water and with cold diethyl ether several times until light yellow precipitate

was obtained. Target compound, 4,7-dibromobenzo[c][1,2,5]thiadiazole, (10.21 g) was achieved with 94% yield. ^1H NMR (400 MHz, CDCl_3) δ 7.68 (s, 2H). ^{13}C NMR (101 MHz, CDCl_3), d (ppm) δ 152.9, 132.4, 113.9.

2.2.2. Synthesis of 3,6-dibromobenzene-1,2-diamine (2)

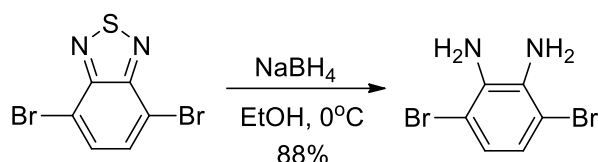


Figure 24. Synthesis of 3,6-dibromobenzene-1,2-diamine

4,7-Dibromobenzo[c][1,2,5]thiadiazole (10.0 g, 34.0 mmol) was dissolved in ethanol (300 mL) at 0 ° C in a 2 L round bottomed flask. To the cooled solution NaBH_4 (25.7 g, 680 mmol) was added in small portions and the mixture was stirred overnight at room temperature. Excess solvent was removed under reduced pressure and resulting solid was extracted with diethyl ether and washed with distilled water four times. Resulting organic phase was dried with MgSO_4 and diethyl ether was evaporated to yield final product as a yellow precipitate (8.0 g, yield 88%).

^1H NMR (400 MHz, CDCl_3) δ 6.85 (s, 2H), 3.91 (s, 4H). ^{13}C NMR (101 MHz, CDCl_3) δ 133.7, 123.3, 109.7.

2.2.3. Synthesis of 4,7-dibromo-2H-benzo[d][1,2,3]triazole (3)

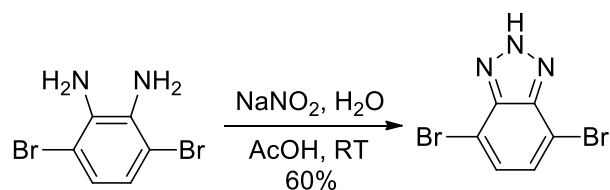


Figure 25. Synthesis of 4,7-dibromo-2H-benzo[d][1,2,3]triazole

To a solution of 3,6-dibromobenzene-1,2-diamine (5.00 g, 18.8 mmol) in acetic acid (85 mL) was added a solution of NaNO₂ (1.43 g, 20.7 mmol) in H₂O (30 mL) slowly. The reaction mixture was stirred at room temperature for an hour. Obtained solids were filtered and washed with water repeatedly. Final compound, 4,7-dibromo-2H-benzo[d][1,2,3]triazole was attained as a pink solid (3.0 g, yield 60%).

2.2.4. Synthesis of 9-(bromomethyl)nonadecane (4)

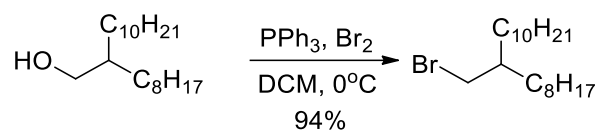


Figure 26. Synthesis of 9-(bromomethyl)nonadecane

A mixture of 2-octyl-1-dodecanol (1.40 g, 4.69 mmol) and triphenylphosphine (PPh₃) (1.25 g, 4.77 mmol) was dissolved in CH₂Cl₂ (20 mL). After the solution was cooled to 0°C, bromine (0.30 mL, 13 mmol) was added dropwise and the resulting mixture was stirred overnight at room temperature. To remove excess bromine, solution was washed with saturated NaHSO₃ solution. Organic layer was washed with distilled water and brine and organic layer was dried over MgSO₄. After evaporation of solvent, obtained product was further purified by silica gel column chromatography using hexane (1.59 g, 94%) to get target compound.

¹H NMR (400 MHz, CDCl₃), d (ppm): 3.37(d, J= 4.7 Hz, 2H), 1.52 (m, 1.48–1.55, 1H), 1.20 (m, 1.26–1.14, 32 H), 0.80 (t, J =6.8 Hz, 6H). ¹³C NMR (101 MHz, CDCl₃), d (ppm): 39.6, 39.5, 32.59, 31.9, 29.8, 29.7, 29.6, 29.5, 29.4, 29.3, 26.6, 22.7, 14.1.

2.2.5. Synthesis of 4,7-dibromo-2-(2-octyldodecyl)-2H-benzo[d][1,2,3]triazole (5)

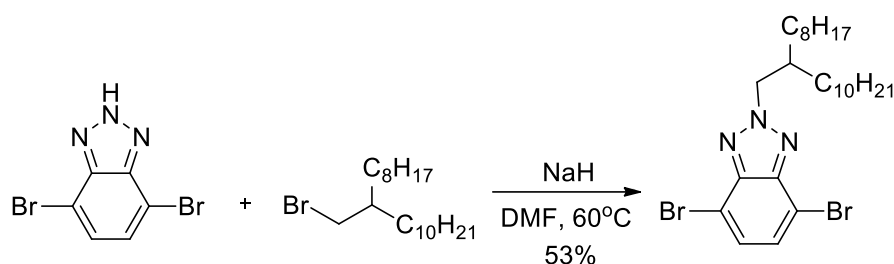


Figure 27. Synthesis of 4,7-dibromo-2-(2-octyldodecyl)-2H-benzo[d][1,2,3]triazole

In an Argon purged flask, 4,7-dibromo-2H-benzo[d][1,2,3]triazole (2.36 g, 8.5 mmol) was dissolved in DMF (10 mL). To the solution, hexane washed NaH (245 mg, 10.2 mmol) was added at 0 °C. After NaH was completely reacted, the temperature of the reaction medium was set to 60°C and 9-(bromomethyl)nonadecane (3.70 g, 10.2 mmol) was added into the reaction mixture. The resulting solution was stirred at the same temperature overnight. Reaction mixture was poured into a CHCl₃ and washed with distilled water. Organic layer was dried over MgSO₄ and solvent was removed under vacuo. For the purification of crude product, silica gel column chromatography was performed with with hexane and chloroform (3:1) as the eluent. Final product, 4,7- dibromo-2-(2-octyldodecyl)-2H-benzo[d][1,2,3]triazole, was obtained as a yellow oil (2.5 g, yield 53%). ¹H NMR (400 MHz, CDCl₃), d (ppm): 7.36 (s, 2H), 4.62 (d, *J*= 7.3 Hz, 2H), 2.26 (m, 1H), 1.15 (m, 32H), 0.80 (m, 6H). ¹³C NMR (101 MHz, CDCl₃), d (ppm): 140.3, 128.2, 106.3, 56.6, 35.3, 29.3, 29.4, 29.3, 29.0, 27.5, 27.3, 27.2, 27.1, 27.0, 26.9, 23.5, 20.4, 20.3, 11.5.

2.2.6. Synthesis of 2,2'-(2-(2-octyldodecyl)-2H-benzo[d][1,2,3]triazole-4,7-diyl)dithiazole (6)

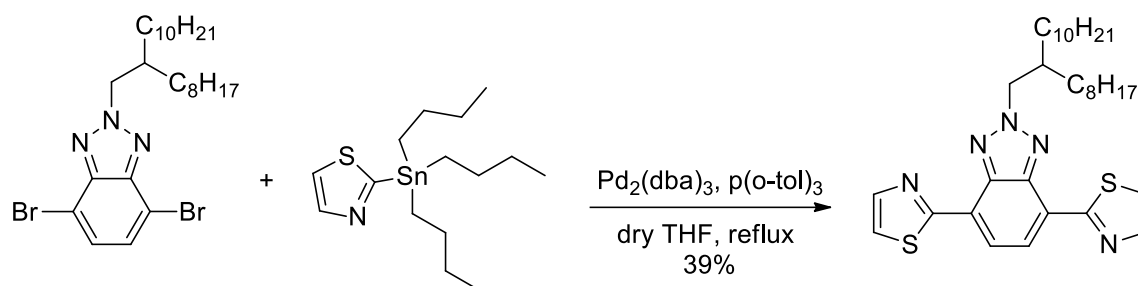


Figure 28. Synthesis of 2,2'-(2-(2-octyldodecyl)-2H-benzo[d][1,2,3]triazole-4,7-diyl)dithiazole

4,7-Dibromo-2-(2-(2-octyldodecyl)-2H-benzo[d][1,2,3]triazole (300 mg, 0.55 mmol) and commercially available 2-(tributylstannyl)thiazole (415 mg, 1.11 mmol) were taken into 50 mL round bottomed flask and dissolved in dry THF (15 mL). After the reaction mixture was subjected to Argon bubbling for an hour, Pd₂(dba)₃ (24 mg, 0.04 mmol) and tri-*o*-tolylphosphine (65 mg, 0.21 mmol) was added. Resulting solution was left to reflux overnight. For purification of the target compound extraction with chloroform and distilled water was performed. Organic layer was dried and the solvent was evaporated. 2,2'-(2-(2-octyldodecyl)-2H-benzo[d][1,2,3]triazole-4,7-diyl)dithiazole was obtained after silica gel column chromatography with chloroform/hexane (4:1.5) solvent system with a yield of 39%. ¹H NMR (400 MHz, CDCl₃), d (ppm): 8.44 (s, 2H), 8.03 (s, 2H), 7.55 (s, 2H), 4.85 (d, *J*= 7.3 Hz, 2H), 3.67 (m, 1H), 1.15 (m, 32H), 0.80 (m, 6H).

2.2.7. Synthesis of 2,2'-(2-(2-octyldodecyl)-2H-benzo[d][1,2,3]triazole-4,7-diyl)bis(5-bromothiazole) (M1) (7)

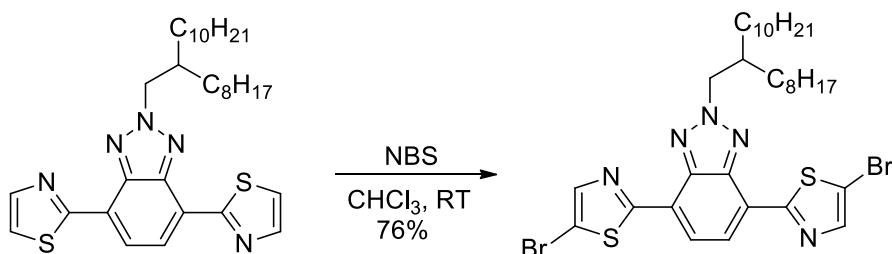


Figure 29. Synthesis of 2,2'-(2-(2-octyldodecyl)-2H-benzo[d][1,2,3]triazole-4,7-diyl)bis(5-bromothiazole)

120 mg of 2,2'-(2-(2-octyldodecyl)-2H-benzo[d][1,2,3]triazole-4,7-diyl)dithiazole was taken up in a 50 mL round bottom flask and dissolved in chloroform (30 mL). To this solution 24 mg of NBS were added slowly and the mixture was stirred overnight. For purification, reaction mixture was extracted with chloroform and organic solvent was removed under reduced pressure. After TLC monitoring target compound was used directly in polymerization without further purification. ¹H NMR (400 MHz, CDCl₃), δ (ppm): 8.37 (s, 2H), 7.89 (s, 2H), 4.81 (d, *J* = 7.3 Hz, 2H), 3.67 (m, 1H), 1.15 (m, 32H), 0.80 (m, 6H).

2.3. Synthesis of Polymers

2.3.1. Synthesis of P1 (8)

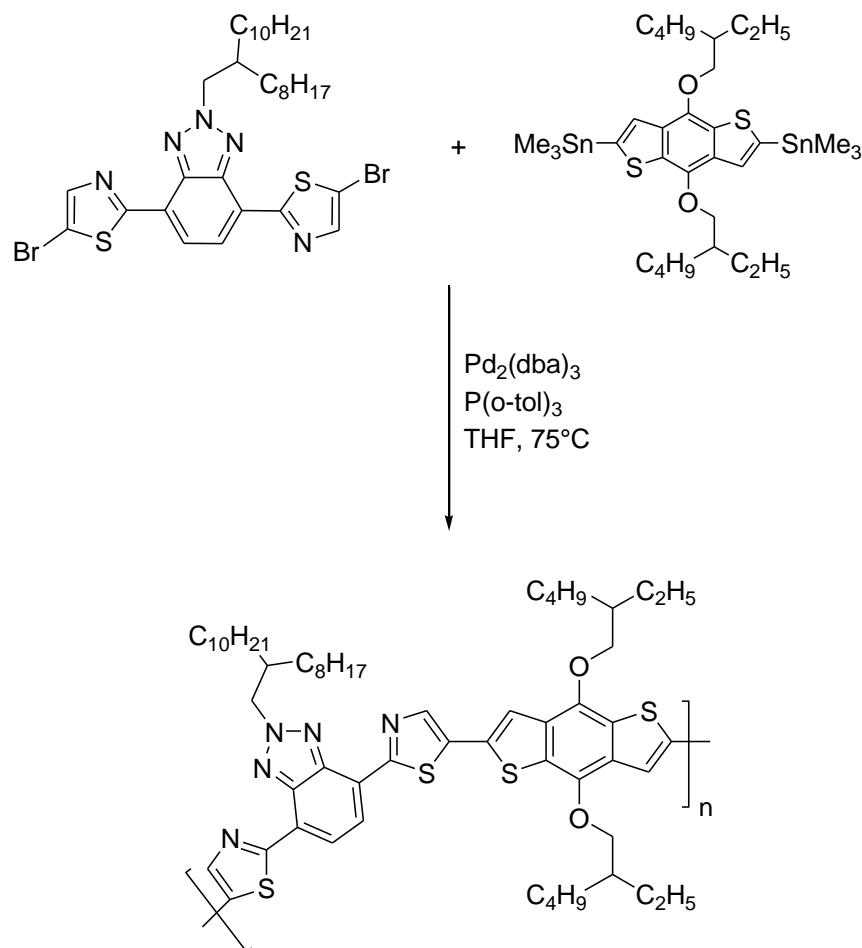


Figure 30. Synthetic Pathway for P1

4,8-Bis((2-ethylhexyl)oxy)benzo[1,2-b:4,5-b']dithiophene-2,6-diylbis(trimethylstannane) (101 mg, 0.131 mmol) and 4,7-bis (5-bromothiazol-2-yl)-2-(2-octyldodecyl)-2H-benzod[1,2,3]triazole (90 mg, 0.13 mmol) were added into 100 mL of two-round bottom flask and purged with argon for about half an hour. Then it was dissolved in 10 mL of THF. $\text{Pd}_2(\text{dba})_3$ (6.32 mg 5% by mol) and tris-o-

tolylphosphine (16.8 mg, 40% by mol) were added into the mixture. The reaction medium was stirred and heated to reflux for 40 h. As the first end-capper 2-bromothiophene (81 mg, 0.5 mmol) was added. 3 h later, 2-tributylstanylthiophene (373 mg, 1.0 mmol) was added as the second end-capper. The reaction mixture was stirred overnight. Then solvent was removed under vacuo. The bulky mixture was dissolved with CHCl_3 and precipitated into methanol. The crude polymer was purified via Soxhlet extraction by using acetone, hexane respectively. Finally, polymer was extracted with CHCl_3 and precipitated with methanol in order to get solid polymer. GPC result of the polymer is as follows: M_w (weight average molecular weight): 32700 Da, M_n (number average molecular weight): 17400 Da, and PDI (polydispersity index) value is 1.87.

2.3.2. Synthesis of P2 (9)

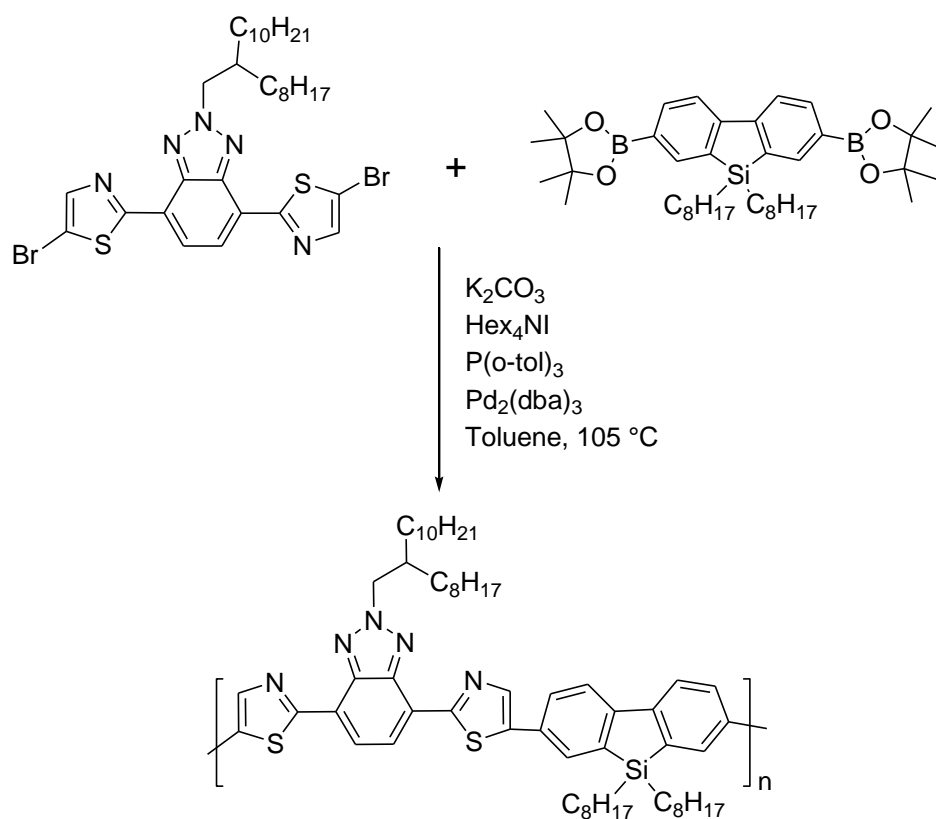


Figure 31. Synthetic Pathway for P2

In a dried 100 mL of two-round bottom flask 2M K₂CO₃ solution (2.34 mL) was added and the medium was purged with inert atmosphere. Then, 9,9-dioctyl-9H-9-silafluorene-2,7-bis(boronic acid pinacol ester) (163 mg, 0.235 mmol) and 4,7-bis (5-bromothiazol-2-yl)-2-(2-octyldodecyl)-2H-benzo[d][1,2,3]triazole (170 mg, 0.247 mmol) were added and purged with argon for additional 30 minutes. Then, freshly dried toluene (10 mL) and catalytic amount of tetrahexyl ammonium iodide were added into reaction medium. Followed by Pd₂(dba)₃ (10.75 mg, 5% by mol) and tris-*o*-tolylphosphine (28.6 mg, 40% by mol). The reaction medium was stirred and heated to reflux for 18 h under argon atmosphere. In order to terminate the polymerization bromobenzene (146.6 mg, 0.94 mmol) was added. 4 h later phenyl boronic acid (229.20 mg, 1.88 mmol) was added as the second end-capper. Then the mixture was stirred at 105 °C overnight. The medium is cooled down to ambient temperature and precipitated in methanol. After filtration step, in order to eliminate oligomers and small molecules soxhlet apparatus was used. Solid polymer was finally purified with CHCl₃ and precipitated in methanol. Pure polymer was dried in vacuo at 40 °C for 24h. GPC result of the polymer is as follows: M_w (weight average molecular weight): 48900 Da, M_n (number average molecular weight): 34500 Da, and PDI (polydispersity index) value is 1.42.

CHAPTER 3

RESULTS & DISCUSSION

3.1. Electrochemical Studies

In renewable energy technologies electrochemical analysis in a quantitative manner has become a significant tool. For this purpose, to measure the current obtained from electrochemical cells, cyclic voltammetry was utilized. In this method characteristic oxidation and reduction properties of the compounds can be determined. Besides, HOMO and LUMO energy levels can be calculated with the same method. With these information in hand, electrochemical studies of **P1** and **P2** were completed by CV techniques to examine both redox behaviors and HOMO–LUMO energy levels of polymers via GAMRY Instrument Potentiostat/ Galvanostat/ZRA at a scan rate of 100 mV/s. Analyses were performed using three electrode system in 0.1 M TBAPF₆ / ACN electrolyte/solvent couple. Polymer/chloroform solution was coated on to ITO surface via spray coating for CV measurements. As indicated in Table 1, **P1** showed p-type doping and de-doping potentials at 1.40 V/0.56 V and n-type doping and de-doping potentials at -1.60 V/-1.44 V, respectively. Similarly, **P2** had p-type doping and de-doping potential at 1.48 V/1.10 V and n-type doping and de-doping potential at -1.76 V/-1.40 V, respectively (Figure 33). From these results, it can be concluded as both polymers have ambipolar characteristics.

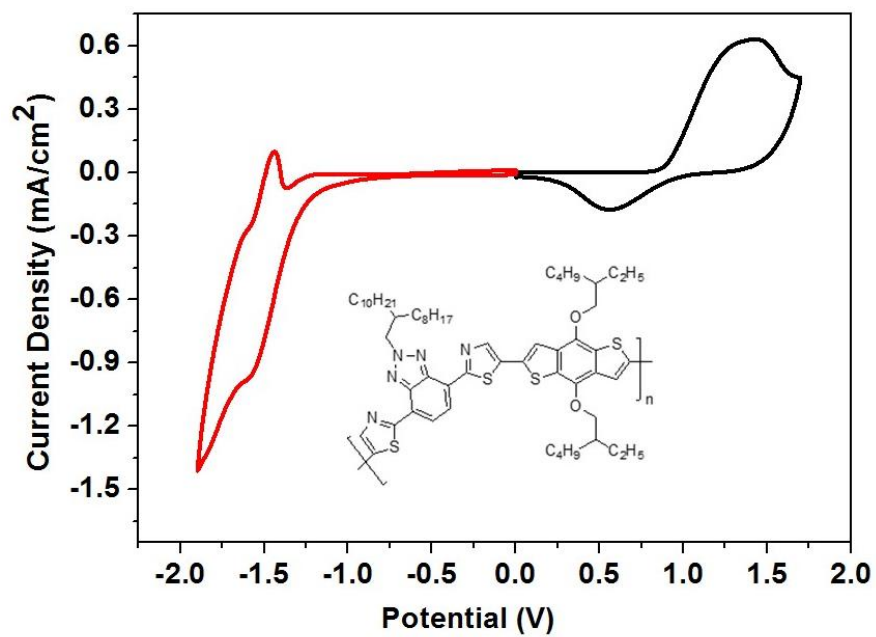


Figure 32. Cyclic Voltammogram of **P1** at a scan rate of 100 mV/s

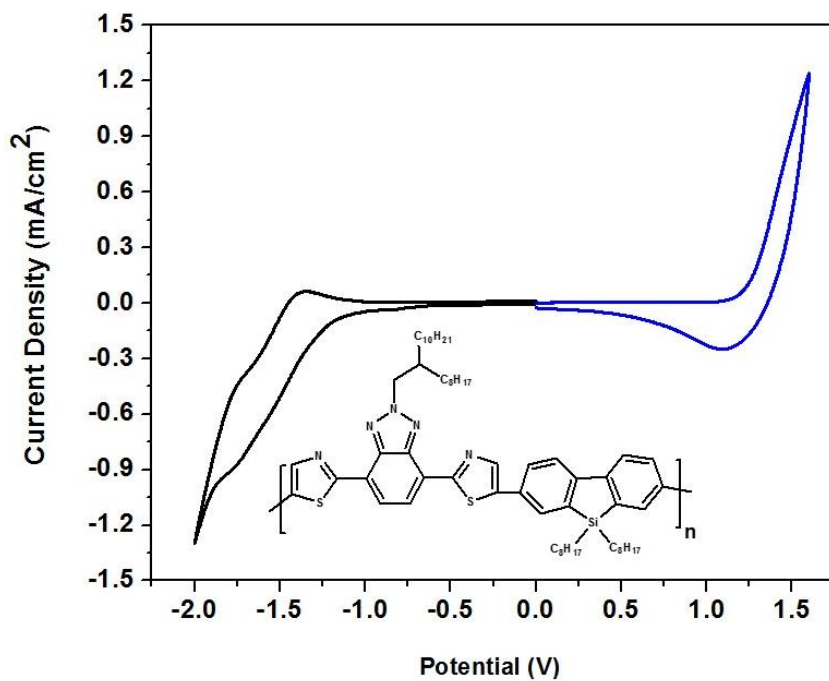


Figure 33. Cyclic Voltammogram of **P2** at a scan rate of 100 mV/s

As it was mentioned in the introduction part, HOMO and LUMO energy levels of the polymers play an important role in device construction. Determination of HOMO and LUMO energy level can be done by using the formulas shown below:

$$E_{HOMO}(eV) = -(4.75 + E_{oxidation, onset})$$

$$E_{LUMO}(eV) = -(4.75 + E_{reduction, onset})$$

To obtain HOMO and LUMO energy levels from these equations, onset oxidation and reduction potentials must be specified. Determination of these values were carried out by drawing tangent lines to the doping peaks. According to the calculations, HOMO and LUMO energy levels of **P1** and **P2** were obtained as -5.63 eV/3.60 eV and -6.0 eV/3.58 eV respectively.

Similarly, electronic band gap of the polymers were calculated with the help of the equation shown below:

$$E_g^{el} = HOMO - LUMO$$

Calculations were resulted that, the electrochemical band gap energy of **P1** and **P2** are 2.03 and 2.42 respectively.

$$E_{LUMO}(eV) = -(4.75 + E_{reduction, onset})$$

$$E_{HOMO}(eV) = -(4.75 + E_{oxidation, onset})$$

The results of the electrochemical studies discussed above were outlined in Table 1.

Table 1. Electrochemical studies of polymer

	$E_{p-doping}$ (V)	$E_{p-dedoping}$ (V)	$E_{n-doping}$ (V)	$E_{n-dedoping}$ (V)	HOMO (eV)	LUMO (eV)	E_g^{op} (eV)	E_g^{el} (eV)
P1	1.40	0.56	-1.60	-1.44	-5.63	-3.60	2.10	2.03
P2	1.48	1.10	-1.76	-1.40	-6.00	-3.58	1.74	2.42

Considering the HOMO-LUMO calculation results, due to the electron donating ability of sulphur atom throughout the ring system benzodithiophene containing polymer **P1** shows high lying HOMO level than silafluorene based polymer **P2**. Thus, band gap energy of the **P1** decreased as expected. Results obtained from the calculation by using HOMO and LUMO energy levels of the polymers were consistent with the situation mentioned above. The electrochemical band gaps of **P1** and **P2** were found as **2.03** and **2.42** respectively.

The other important parameter to achieve efficient charge transfer is LUMO energy level. Since we use PC₇₁BM as the acceptor in solar cell applications, theoretically LUMO energy level difference of the chemically synthesized polymers and PC₇₁BM (LUMO: -3.91 eV) should be in the range of 0.3-0.5 eV in order to obtain high solar cell efficiency. LUMO energy level of **P1** and **P2** was measured as -3.60 eV, -3.58 eV respectively which were in proper range.

3.2. Spectroelectrochemical Properties

The electronic and optical responses were analyzed by spectroelectrochemical methods. By applying incremental potential, responses of the polymers were investigated with the help of UV-VIS spectroscopy. For this purpose, chemically synthesized polymers were dissolved using chloroform. Polymers were coated on ITO coated glass electrodes by spray coating method then they were dipped into 0.1 M TBAPF₆/ACN solution. Absorption properties were examined between range of 0 V and 1.4 V for **P1**, 0 V and 1.5 V for **P2**.

As seen in Figure 34 and Figure 35, 500 and 544 nm are observed as the neutral state absorption wavelengths for **P1** and 490 nm was observed as neutral state absorption peak for **P2**. Visible range absorptions indicated that the π - π^* inter-band transitions. According to the difference between absorbed wavelengths, **P1** showed red shift with respect to **P2**. This might be due to the electron rich chemical structure of BDT unit.

Besides, during this application, except for the neutral absorption bands, the new bands were observed at 765 nm and 1315 nm which show the existence of polaronic and bipolaronic carriers at polymer backbone for **P1**.

For the compatibility to the OPV applications, the band gap is the crucial factor for better efficiency. λ_{onset} of the absorption wavelengths were used for the calculation of optical band gaps of the polymers, which were 2.10 and 1.74 eV for **P1** and **P2** respectively. Results were summarized in Table 2

Table 2. Summary of the spectroelectrochemical studies

	λ_{onset} (nm)	E_g^{op} (eV)
P1	590	2.10
P2	713	1.74

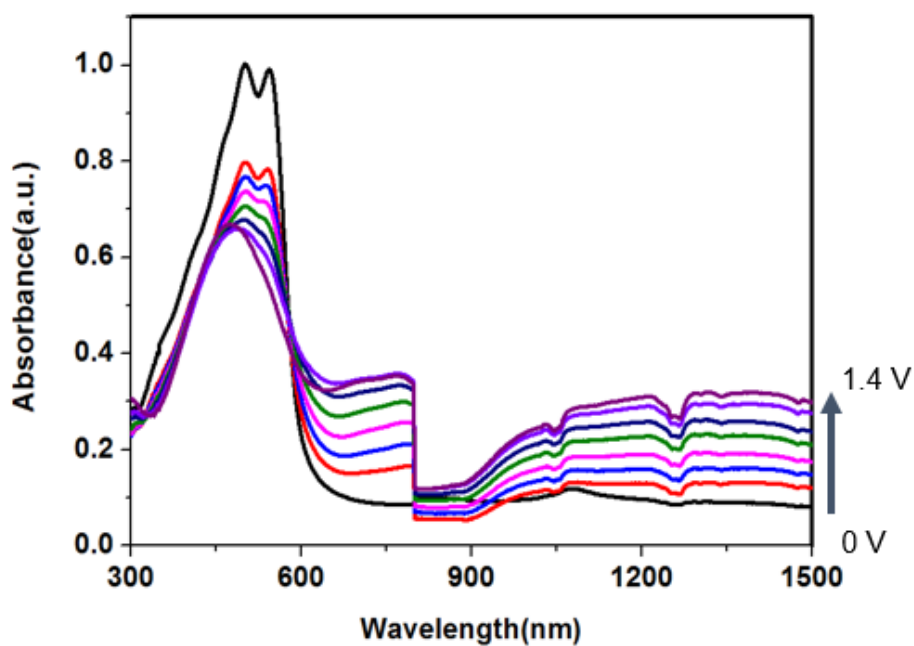


Figure 34. Electronic absorption spectra of the **P1** in UV-Vis-NIR regions

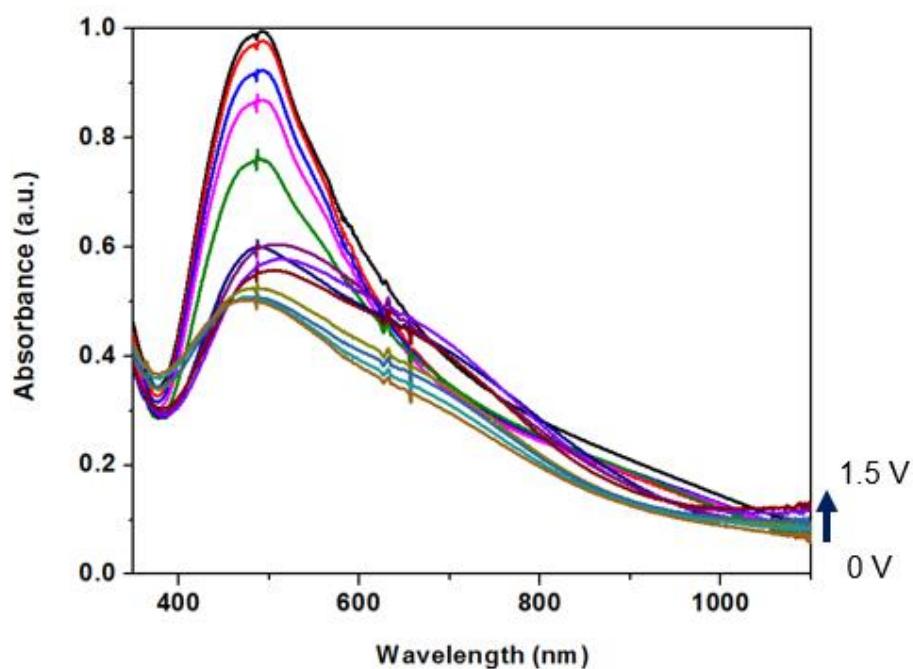


Figure 35. Electronic absorption spectra of the **P2** in UV-Vis-NIR regions

3.3. Kinetic Studies

To demonstrate the transmittance change with respect to time kinetic studies were performed. In this respect, maximum wavelengths that polymers absorbed were picked.

Transmittance (ΔT %) change and switching time properties of **P1** and **P2** were studied by alternating oxidation/reduction method with a time interval of 5 seconds. Optical contrast values were defined at which polymers show the highest absorbance in the spectrum. As a result, **P1** showed 7%, 40% and 27% optical contrasts at 500 nm, 765 nm and 1315 nm respectively. **P2** showed 11% optical contrast at 490 nm. The optical contrast and switching time responses of the polymers were summed up in Table 3.

Table 3. Optical Contrast and Switching Times of P1 and P2

Polymer	Wavelength (nm)	Optical contrast (ΔT %)	Switching times (s)
P1	500	7	0.6
	765	40	0.9
	1315	27	0.8
P2	490	11	2.8

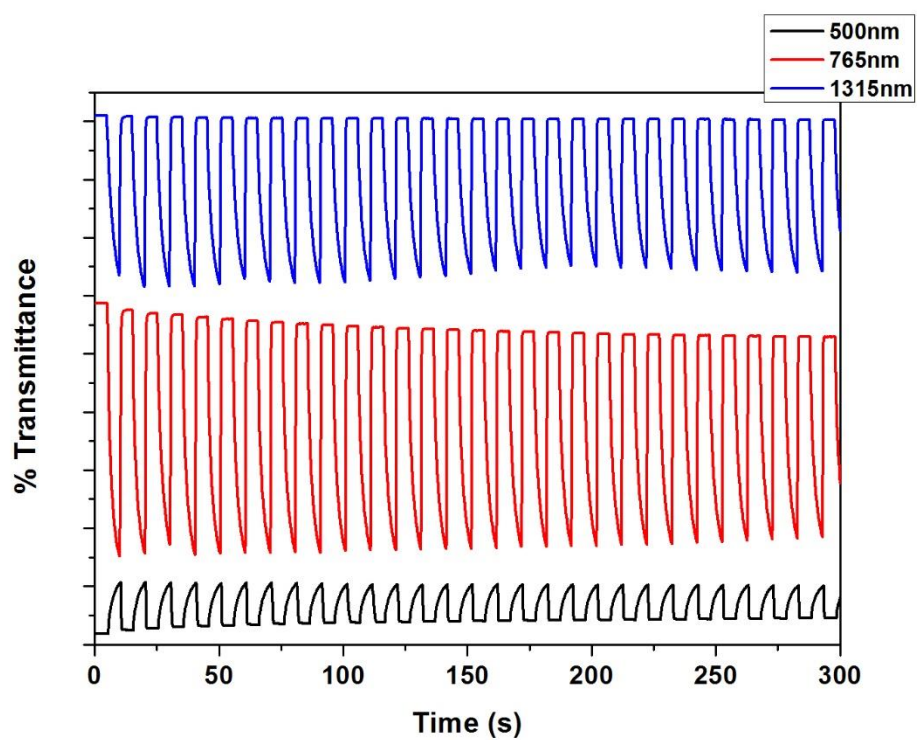


Figure 36. Percent Transmittance change for P1 at 500, 765 and 1315 nm

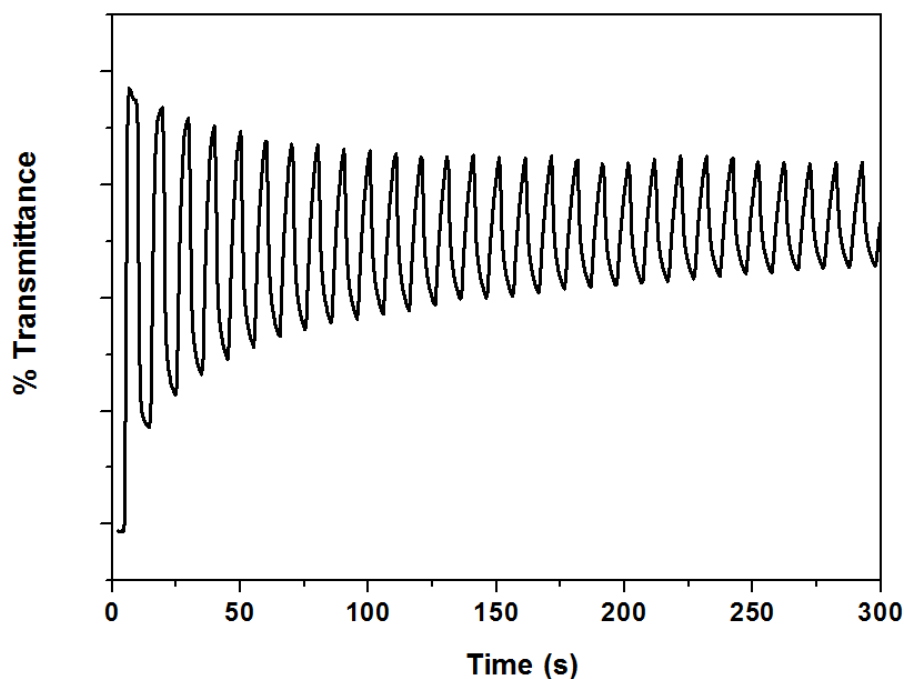


Figure 37. Percent Transmittance change for **P2** at 490nm

3.4. Thermal Analysis

Thermal studies were done by thermogravimetry analyses (TGA) and differential scanning calorimetry (DSC). TGA was performed under N₂ atmosphere and the heating rate was 10 °C/min. 5% mass loss was seen at 178 °C for **P1** and 225 °C for **P2**. Glass transition temperature was not observed for both **P1** and **P2**. TGA and DSC analysis results were shown in Appendix part.

3.5. Photovoltaic Studies

Two new donor polymers, **P1** and **P2**, were blended with fullerene acceptor and were used in the organic solar cell device. For organic solar cell applications, conventional device architecture ITO/ PEDOT:PSS/ Polymer:PCBM /LiF/Al was used. Current density vs voltage characteristics of device were monitored under AM 1.5G illumination at room temperature (Figure 38-39). Polymer-fullerene ratios (w/w)

short-circuit current density, open-circuit voltage, fill factor, and power conversion efficiencies of the constructed devices were examined. Optimization studies for **P1** and **P2** were performed by changing polymer-fullerene ratios (w/w) in order to decide on the conditions that result in highest efficiency. As the amount of PC₇₀BM increases, the efficiency of electron transportation also increases which has reflected in better PCE and short circuit current. On the other hand, decreasing the amount of polymer may result in the decrease of short circuit current and PCE due to the lowered amount of collected photons.

With these in hand, the best results obtained from both polymers were summarized in Table 4.

Table 4. Photovoltaic studies based on **P1** and **P2**

P1:PC₇₀BM	J_{sc}	V_{oc}	I_{max}	V_{max}	$FF(\%)$	PCE	<i>Treatment</i>
1:1	2.03	0.49	1.28	0.27	35	0.35	-
1:2	2.53	0.49	1.59	0.27	35	0.43	-
1:3	2.57	0.49	1.93	0.21	32	0.40	-
1:4	2.68	0.49	1.71	0.26	34	0.45	-
1:4	2.10	0.44	1.21	0.25	33	0.30	500 rpm
1:4	1.81	0.43	1.02	0.25	32	0.25	1000 rpm
P2:PC₇₀BM							
1:2	1.37	0.49	0.89	0.29	38	0.26	750 rpm
1:3	1.03	0.51	0.65	0.30	37	0.19	750 rpm

As seen in Table 4, short circuit current and PCE were observed to have parallel trends with PCBM ratio. As a result, electron transport capacity increases with higher PCBM amount. In contrast to **P1**, **P2** short circuit current and results were decreased with the increasing PCBM ratio. This opposing outcomes may be linked to the morphology of

P2. V_{oc} values were obtained as 0.43 - 0.49 V for **P1** and 0.49-0.51 V for **P2**. Even if **P2** has higher V_{oc} compared to **P1**, short circuit current (J_{sc}) values are more decisive in the PCE values.

Fill factor (FF) values of **P1** and **P2** were calculated from current density – voltage curves were obtained under AM 1.5G simulated solar illumination at 100 mW/cm². FF values were found to be 32-35 % and 37-38 % for **P1** and **P2** respectively (Figure 38-39).

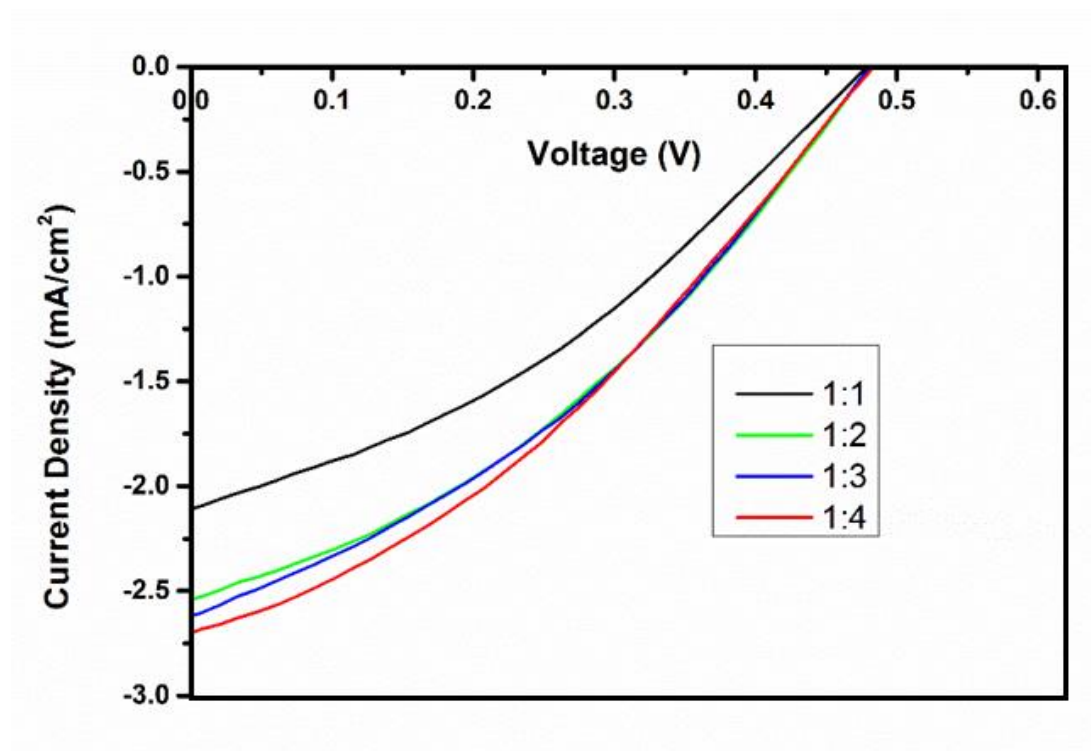


Figure 38. I-V characteristics of photovoltaic devices based on **PI:PCBM(1:4)**, **PI:PCBM(1:3)**, **PI:PCBM(1:2)**, **PI:PCBM(1:1)** blends.

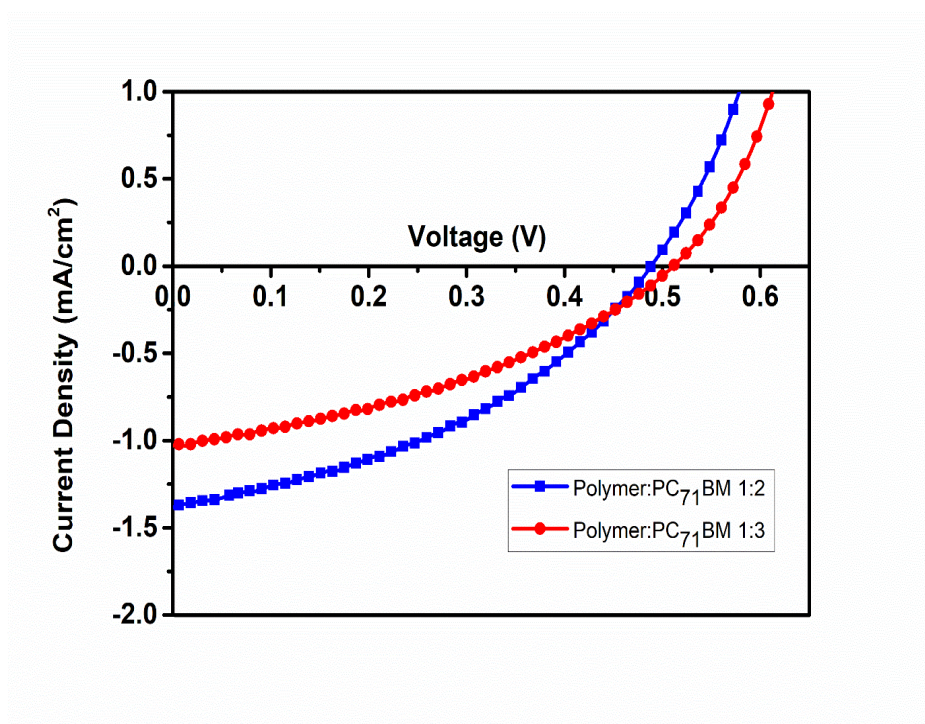


Figure 39. I-V characteristics of photovoltaic devices based on **P2**:PCBM(1:3), **P2**:PCBM(1:2) blends.

3.6. Optical Studies

The UV-Vis spectra results of **P1** and **P2** are shown in Figure 40-41. **P1** demonstrated two maximum absorption peaks. This might be related to π - π^* transition and intermolecular charge transfer. Thin film form of the **P1** showed red shift absorbance spectra. Intermolecular π - π stacking at thin film form causes red shift of the spectra.

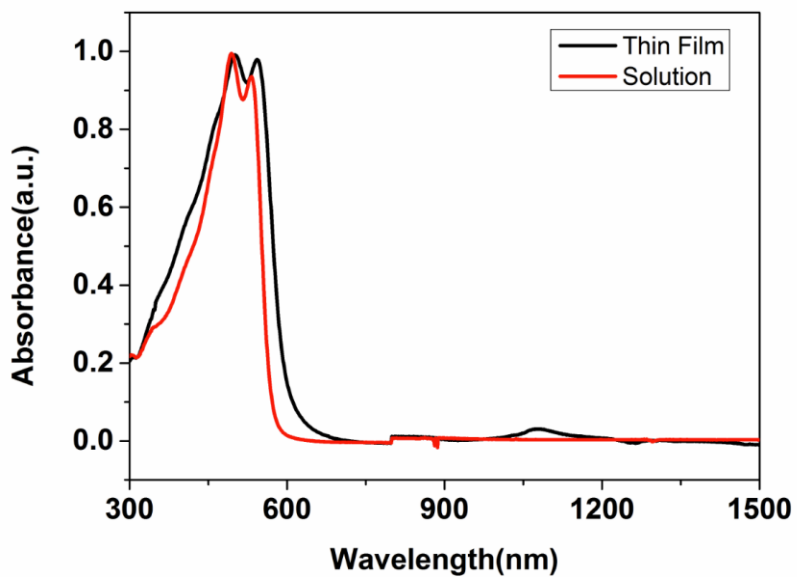


Figure 40. Absorbance spectra of **P1**

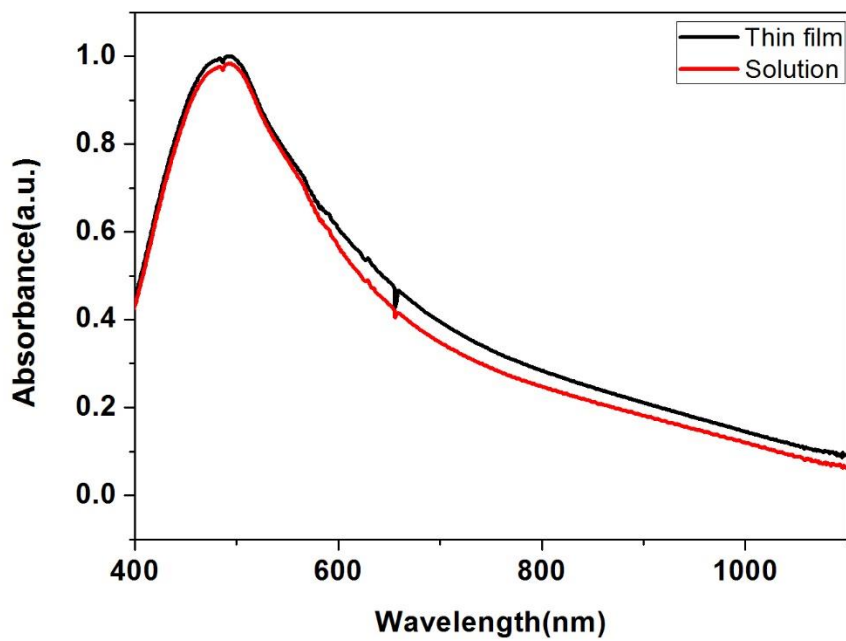


Figure 41. Absorbance spectra of **P2**

CHAPTER 4

CONCLUSIONS

Due to the functional utility of solar cells two polymers, **P1** and **P2**, having different donor groups were designed, synthesized and characterized. During the design, donor-acceptor-donor approach was used as a key process. Synthesis of monomer having acceptor feature was based on the Stille Coupling reaction. For this purpose, benzothiadiazole derivative was converted to corresponding dibromotriazole unit. For the solubility adjustment 9-(bromoethyl)nonadecane unit was attached to the dibromotriazole. For coupling reaction, commercially available 2-(tributylstannyl)thiazole and dibromotriazole unit were reacted with each other to obtain corresponding acceptor unit. From this point, two different donors were connected with the synthesized acceptor moiety to investigate optoelectronic properties of obtained polymers **P1** and **P2**. As a donor unit polymer **P1** included **BDT**; while **P2** contain silafluorene unit.

In organic solar cell construction **P1** and **P2** were used as the active layer and blending with PC₇₀BM to get bulk heterojunction. According to electrochemical studies both polymers have n-dopable and p-dopable nature. The optical band gap of polymers were calculated as 2.10 eV and 1.74 eV using λ_{onset} values which were 590 nm and 713 nm respectively. According to electrochemical studies, HOMO and LUMO levels were proper for organic solar cell applications. Similarly, optical measurements of the polymers showed that, band gap values of them was suitable for device construction. Device construction was carried out by using conventional solar cell structure. To maximize the interface surface area to volume ratio, BHJ method was utilized and device was constructed according to ITO/ PEDOT: PSS/ polymer: PC₇₀BM/ LiF/ Al design. By using these two devices, current density voltage characteristics were examined under AM 1.5G illumination. Power conversion efficiency of devices were

measured as 0.45% for **P1** and 0.26% for **P2**. V_{oc} and J_{sc} of **P1** was obtained as 0.49 V and 2.68 mA/cm² respectively when device showed maximum PCE with FF of 34 %. Furthermore, we measured the best PCE for **P2** at V_{oc} of 0.49 V and J_{sc} of 1.37 mA/cm² with FF of 38 %.

REFERENCES

- (1) Lee, N. A.; Gilligan, G. E.; Rochford, J. Solar Energy Conversion. *Green Chem. An Incl. Approach* **2017**, *60* (3), 881–918. <https://doi.org/10.1016/B978-0-12-809270-5.00030-3>.
- (2) Becquerel E. Memoire Sure Les Effets Electriques Produits Ous l'influence Des Rayons Solaires. *Comptes Rendues* **1839**, *6*, 561–567.
- (3) Einstein, A. Über Einen Die Erzeugung Und Verwandlung Des Lichtes Betreffenden Heuristischen Gesichtspunkt [AdP 17, 132 (1905)]. *Ann. Phys.* **2005**, *14* (S1), 164–181. <https://doi.org/10.1002/andp.200590004>.
- (4) Arons, A. B.; Peppard, M. B. Einstein's Proposal of the Photon Concept—a Translation of the Annalen Der Physik Paper of 1905. *Am. J. Phys.* **1965**, *33* (5), 367–374. <https://doi.org/10.1119/1.1971542>.
- (5) Millikan, R. A. A Direct Photoelectric Determination of Planck's " h " . *Phys. Rev.* **1916**, *7* (3), 355–388. <https://doi.org/10.1103/physrev.7.355>.
- (6) Millikan, R. A. A Direct Determination of " H ." . *Phys. Rev.* **1914**, *4* (1), 73–75. <https://doi.org/10.1103/physrev.4.73.2>.
- (7) Tadesse, T. Application of Conjugated Organic Polymers for Photovoltaic's: Review. *J. Phys. Chem. Biophys.* **2018**, *08* (01), 1–6. <https://doi.org/10.4172/2161-0398.1000263>.
- (8) Chapin, D. M.; Fuller, C. S.; Pearson, G. L. A New Silicon P-n Junction Photocell for Converting Solar Radiation into Electrical Power [3]. *J. Appl. Phys.* **1954**, *25* (5), 676–677. <https://doi.org/10.1063/1.1721711>.
- (9) Shockley, W.; Queisser, H. J. Detailed Balance Limit of Efficiency of P-n Junction Solar Cells. *J. Appl. Phys.* **1961**, *32* (3), 510–519. <https://doi.org/10.1063/1.1736034>.
- (10) Rühle, S. Tabulated Values of the Shockley-Queisser Limit for Single Junction Solar Cells. *Sol. Energy* **2016**, *130*, 139–147. <https://doi.org/10.1016/j.solener.2016.02.015>.
- (11) Tabachnyk, M.; Musser, A.; Rao, A. Beyond the Shockley-Queisser Limit with Singlet Exciton Fission. *SPIE Newsroom* **2015**, 3–5. <https://doi.org/10.1117/2.1201506.005985>.
- (12) Rao, A.; Friend, R. H. Harnessing Singlet Exciton Fission to Break the Shockley-Queisser Limit. *Nat. Rev. Mater.* **2017**, *2* (11), 17063. <https://doi.org/10.1038/natrevmats.2017.63>.

- (13) Tanabe, K. A Review of Ultrahigh Efficiency III-V Semiconductor Compound Solar Cells: Multijunction Tandem, Lower Dimensional, Photonic up/down Conversion and Plasmonic Nanometallic Structures. *Energies*. July **2009**, 504–530. <https://doi.org/10.3390/en20300504>.
- (14) Khaledi-Nasab, A.; Sabaeian, M.; Sahrai, M.; Fallahi, V. Kerr Nonlinearity Due to Intersubband Transitions in a Three-Level InAs/GaAs Quantum Dot: The Impact of a Wetting Layer on Dispersion Curves. *J. Opt. (United Kingdom)* **2014**, *16* (5), 055004. <https://doi.org/10.1088/2040-8978/16/5/055004>.
- (15) Green, M. A. Third Generation Photovoltaics: Solar Cells for 2020 and Beyond. *Phys. E Low-Dimensional Syst. Nanostructures* **2002**, *14* (1–2), 65–70. [https://doi.org/10.1016/S1386-9477\(02\)00361-2](https://doi.org/10.1016/S1386-9477(02)00361-2).
- (16) Semonin, O. E.; Luther, J. M.; Choi, S.; Gao, J.; Chen, H.-Y.; Beard, M. C.; Nozik, A. J. Multiple Exciton Generation in PbSe Quantum Dot Solar Cells. *SPIE* **2011**, *2* (17063), <https://doi.org/10.1117/2.1201203.004146> Multiple.
- (17) Sabaeian, M.; Khaledi-Nasab, A. Size-Dependent Intersubband Optical Properties of Dome-Shaped InAs/GaAs Quantum Dots with Wetting Layer. *Appl. Opt.* **2012**, *51* (18), 4176. <https://doi.org/10.1364/ao.51.004176>.
- (18) Pietryga, J. M.; Park, Y. S.; Lim, J.; Fidler, A. F.; Bae, W. K.; Brovelli, S.; Klimov, V. I. Spectroscopic and Device Aspects of Nanocrystal Quantum Dots. *Chem. Rev.* **2016**, *116* (18), 10513–10622. <https://doi.org/10.1021/acs.chemrev.6b00169>.
- (19) Smith, M. B.; Michl, J. Singlet Fission. *Chem. Rev.* **2010**, *110* (11), 6891–6936. <https://doi.org/10.1021/cr1002613>.
- (20) Greyson, E. C.; Vura-Weis, J.; Michl, J.; Ratner, M. A. Maximizing Singlet Fission in Organic Dimers: Theoretical Investigation of Triplet Yield in the Regime of Localized Excitation and Fast Coherent Electron Transfer. *J. Phys. Chem. B* **2010**, *114* (45), 14168–14177. <https://doi.org/10.1021/jp907392q>.
- (21) Liu, F.; Wang, W.; Wang, L.; Yang, G. Working Principles of Solar and Other Energy Conversion Cells. *Nanomater. Energy* **2012**, *2* (1), 3–10. <https://doi.org/10.1680/nme.12.00024>.
- (22) Hegedus, S. S.; Luque, A. Status, Trends, Challenges and the Bright Future of Solar Electricity from Photovoltaics. In *Handbook of Photovoltaic Science and Engineering*; John Wiley & Sons, Ltd: Chichester, UK, 2005; pp 1–43. <https://doi.org/10.1002/0470014008.ch1>.
- (23) Sproul, A. Understanding the P-n Junction. In *Solar Cells Resources for the Secondary Science Teacher*; UNSW Photovoltaics, 2003; pp 13–24.
- (24) Kelley, T. W.; Baude, P. F.; Gerlach, C.; Ender, D. E.; Muyres, D.; Haase, M. A.; Vogel, D. E.; Theiss, S. D. Recent Progress in Organic Electronics:

- Materials, Devices, and Processes. *Chem. Mater.* **2004**, *16* (23), 4413–4422. <https://doi.org/10.1021/cm049614j>.
- (25) Tang, C. W.; Albrecht, A. C. Transient Photovoltaic Effects in Metal-Chlorophyll-a-Metal Sandwich Cells. *J. Chem. Phys.* **1975**, *63* (2), 953–961. <https://doi.org/10.1063/1.431403>.
- (26) Tang, C. W. Two-Layer Organic Photovoltaic Cell. *Appl. Phys. Lett.* **1986**, *48* (2), 183–185. <https://doi.org/10.1063/1.96937>.
- (27) Hoppe, H.; Sariciftci, N. S. Organic Solar Cells: An Overview. *J. Mater. Res.* **2004**, *19* (7), 1924–1945. <https://doi.org/10.1557/jmr.2004.0252>.
- (28) Rhaman, M. M.; Matin, M. A. Organic Solar Cells: Historical Developments and Challenges. In *Proceedings of 2015 3rd International Conference on Advances in Electrical Engineering, ICAEE 2015*; IEEE, 2016; pp 26–29. <https://doi.org/10.1109/ICAEE.2015.7506788>.
- (29) Luque, A.; Hegedus, S. *Handbook of Photovoltaic Science and Engineering*; 2011. <https://doi.org/10.1002/9780470974704>.
- (30) Scharber, M. C.; Sariciftci, N. S. Efficiency of Bulk-Heterojunction Organic Solar Cells. *Prog. Polym. Sci.* **2013**, *38* (12), 1929–1940. <https://doi.org/10.1016/j.progpolymsci.2013.05.001>.
- (31) Peumans, P.; Yakimov, A.; Forrest, S. R. Small Molecular Weight Organic Thin-Film Photodetectors and Solar Cells. *J. Appl. Phys.* **2003**, *93* (7), 3693–3723. <https://doi.org/10.1063/1.1534621>.
- (32) Brabec, C. J.; Zerza, G.; Cerullo, G.; De Silvestri, S.; Luzzati, S.; Hummelen, J. C.; Sariciftci, S. Tracing Photoinduced Electron Transfer Process in Conjugated Polymer/Fullerene Bulk Heterojunctions in Real Time. *Chem. Phys. Lett.* **2001**, *340* (3–4), 232–236. [https://doi.org/10.1016/S0009-2614\(01\)00431-6](https://doi.org/10.1016/S0009-2614(01)00431-6).
- (33) Brédas, J. L.; Beljonne, D.; Coropceanu, V.; Cornil, J. Charge-Transfer and Energy-Transfer Processes in π -Conjugated Oligomers and Polymers: A Molecular Picture. *Chem. Rev.* **2004**, *104* (11), 4971–5003. <https://doi.org/10.1021/cr040084k>.
- (34) Roncali, J. Synthetic Principles for Bandgap Control in Linear π -Conjugated Systems. *Chem. Rev.* **1997**, *97* (1), 173–206. <https://doi.org/10.1021/cr950257t>.
- (35) McCulloch, I.; Ashraf, R. S.; Biniek, L.; Bronstein, H.; Combe, C.; Donaghey, J. E.; James, D. I.; Nielsen, C. B.; Schroeder, B. C.; Zhang, W. Design of Semiconducting Indacenodithiophene Polymers for High Performance Transistors and Solar Cells. *Acc. Chem. Res.* **2012**, *45* (5), 714–722. <https://doi.org/10.1021/ar200208g>.

- (36) Zhou, H.; Yang, L.; You, W. Rational Design of High Performance Conjugated Polymers for Organic Solar Cells. *Macromolecules* **2012**, *45* (2), 607–632. <https://doi.org/10.1021/ma201648t>.
- (37) Wang, H. J.; Chen, C. P.; Jeng, R. J. Polythiophenes Comprising Conjugated Pendants for Polymer Solar Cells: A Review. *Materials (Basel)*. **2014**, *7* (4), 2411–2439. <https://doi.org/10.3390/ma7042411>.
- (38) Po, R.; Maggini, M.; Camaioni, N. Polymer Solar Cells: Recent Approaches and Achievements. *J. Phys. Chem. C* **2010**, *114* (2), 695–706. <https://doi.org/10.1021/jp9061362>.
- (39) Kroon, R.; Lenes, M.; Hummelen, J. C.; Blom, P. W. M.; De Boer, B. *Small Bandgap Polymers for Organic Solar Cells (Polymer Material Development in the Last 5 Years)*; 2008; Vol. 48. <https://doi.org/10.1080/15583720802231833>.
- (40) Thompson, B. C.; Fréchet, J. M. J. Polymer-Fullerene Composite Solar Cells. *Angew. Chemie - Int. Ed.* **2008**, *47* (1), 58–77. <https://doi.org/10.1002/anie.200702506>.
- (41) Bredas, J. L. Molecular Understanding of Organic Solar Cells: The Challenges. *AIP Conf. Proc.* **2013**, *1519* (11), 55–58. <https://doi.org/10.1063/1.4794709>.
- (42) Helgesen, M.; Søndergaard, R.; Krebs, F. C. Advanced Materials and Processes for Polymer Solar Cell Devices. *J. Mater. Chem.* **2010**, *20* (1), 36–60. <https://doi.org/10.1039/b913168j>.
- (43) Hains, A. W.; Liang, Z.; Woodhouse, M. A.; Gregg, B. A. Molecular Semiconductors in Organic Photovoltaic Cells. *Chem. Rev.* **2010**, *110* (11), 6689–6735. <https://doi.org/10.1021/cr9002984>.
- (44) Dou, L.; You, J.; Yang, J.; Chen, C. C.; He, Y.; Murase, S.; Moriarty, T.; Emery, K.; Li, G.; Yang, Y. Tandem Polymer Solar Cells Featuring a Spectrally Matched Low-Bandgap Polymer. *Nat. Photonics* **2012**, *6* (3), 180–185. <https://doi.org/10.1038/nphoton.2011.356>.
- (45) Jiang, J. M.; Yang, P. A.; Chen, H. C.; Wei, K. H. Synthesis, Characterization, and Photovoltaic Properties of a Low-Bandgap Copolymer Based on 2,1,3-Benzoxadiazole. *Chem. Commun.* **2011**, *47* (31), 8877–8879. <https://doi.org/10.1039/c1cc12040a>.
- (46) Chen, H. Y.; Hou, J.; Zhang, S.; Liang, Y.; Yang, G.; Yang, Y.; Yu, L.; Wu, Y.; Li, G. Polymer Solar Cells with Enhanced Open-Circuit Voltage and Efficiency. *Nat. Photonics* **2009**, *3* (11), 649–653. <https://doi.org/10.1038/nphoton.2009.192>.
- (47) Zhou, H.; Yang, L.; Stuart, A. C.; Price, S. C.; Liu, S.; You, W. Development of Fluorinated Benzothiadiazole as a Structural Unit for a Polymer Solar Cell of 7% Efficiency. *Angew. Chemie - Int. Ed.* **2011**, *50* (13), 2995–2998.

<https://doi.org/10.1002/anie.201005451>.

- (48) He, Z.; Zhong, C.; Su, S.; Xu, M.; Wu, H.; Cao, Y. Enhanced Power-Conversion Efficiency in Polymer Solar Cells Using an Inverted Device Structure. *Nat. Photonics* **2012**, *6* (9), 591–595. <https://doi.org/10.1038/nphoton.2012.190>.
- (49) Li, H.; Xiao, Z.; Ding, L.; Wang, J. Thermostable Single-Junction Organic Solar Cells with a Power Conversion Efficiency of 14.62%. *Sci. Bull.* **2018**, *63* (6), 340–342. <https://doi.org/10.1016/j.scib.2018.02.015>.

APPENDICES

NMR DATA

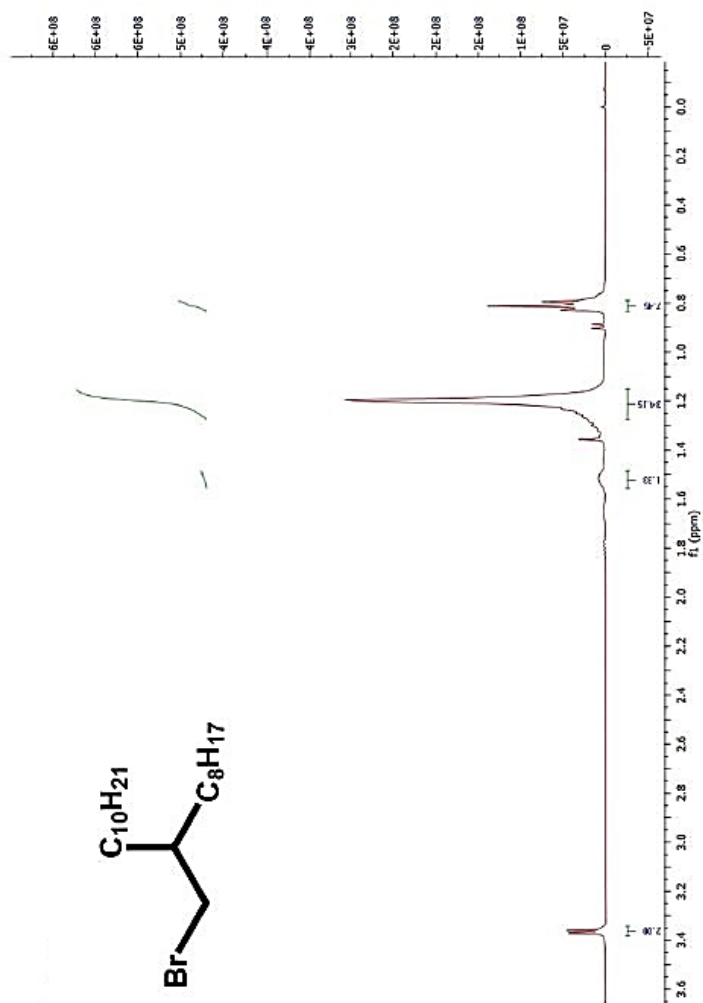


Figure 42. 1H NMR result of 9-(bromomethyl)nonadecane

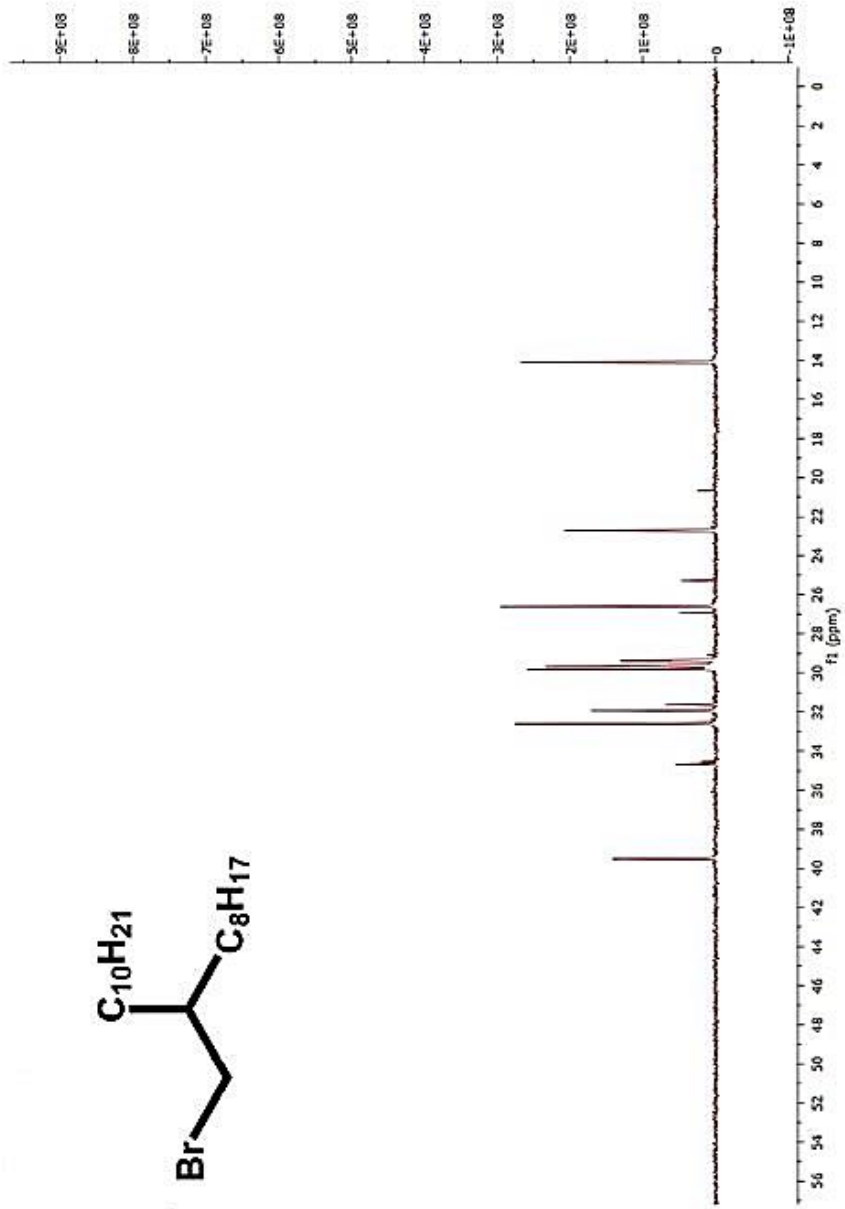


Figure 43. ^{13}C NMR result of 9-(bromomethyl)nonadecane

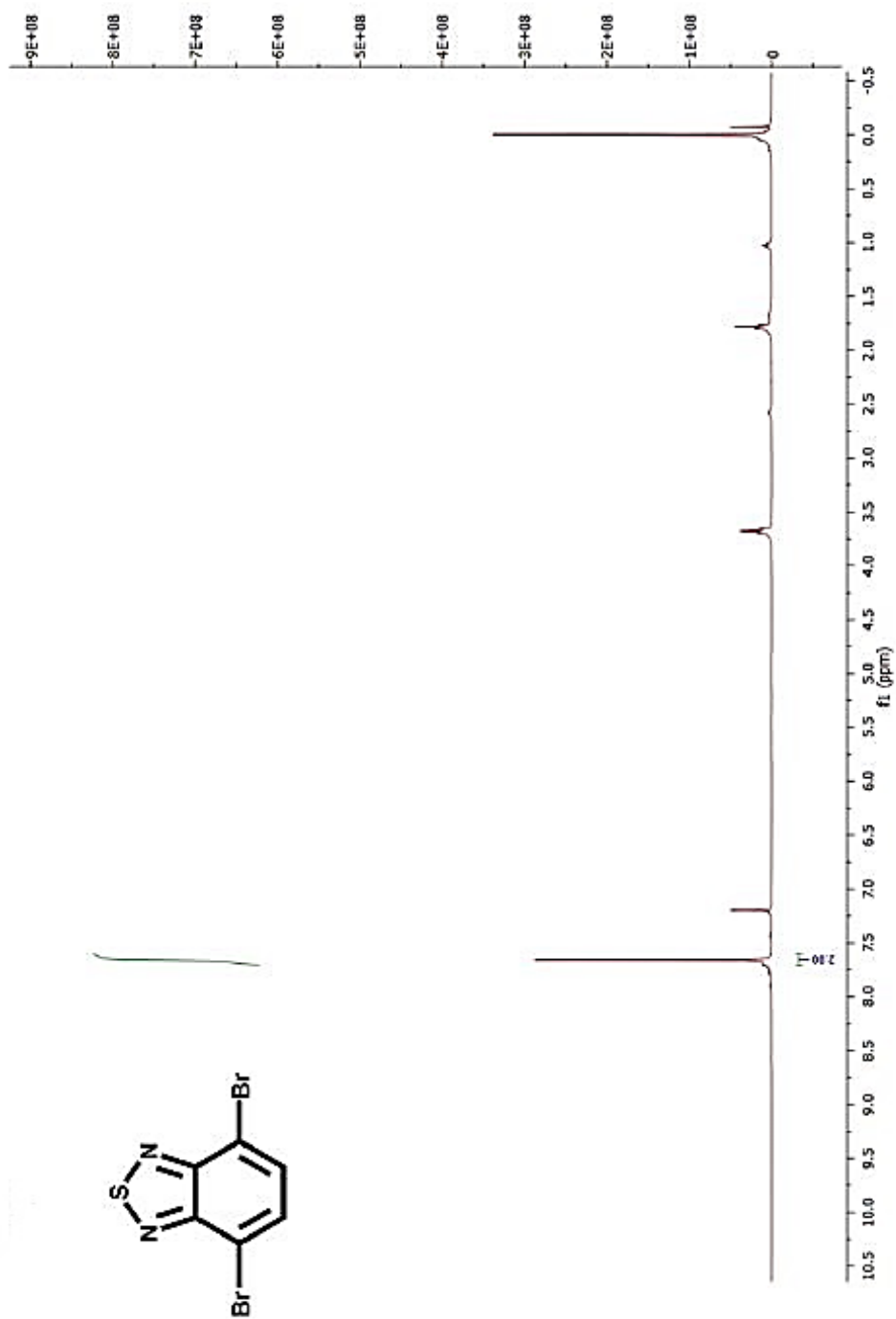


Figure 44. ¹H NMR result of 4,7-dibromobenzo[c][1,2,5]thiadiazole

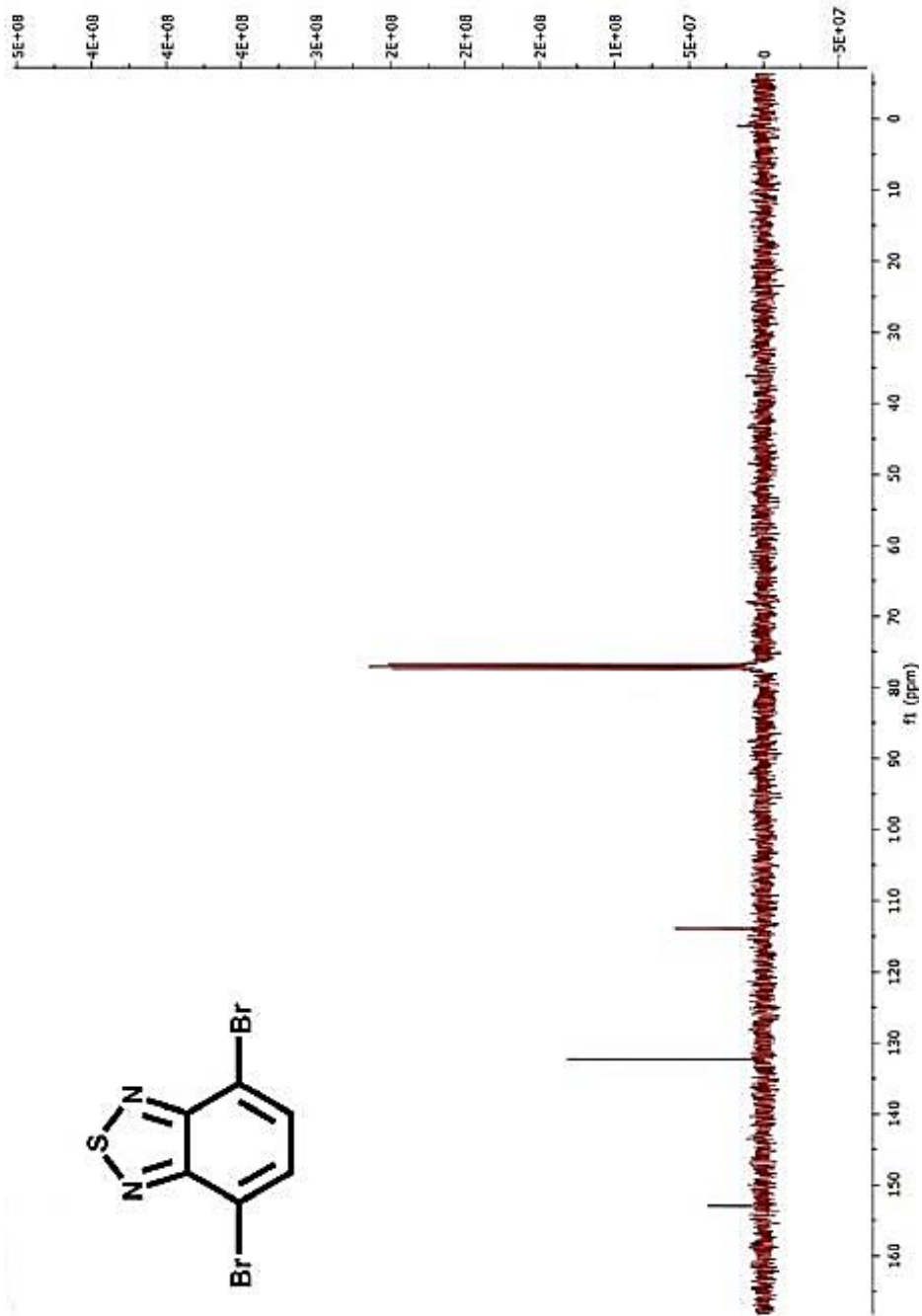


Figure 45. ^{13}C NMR result of 4,7-dibromobenzoc[1,2,5]thiadiazole

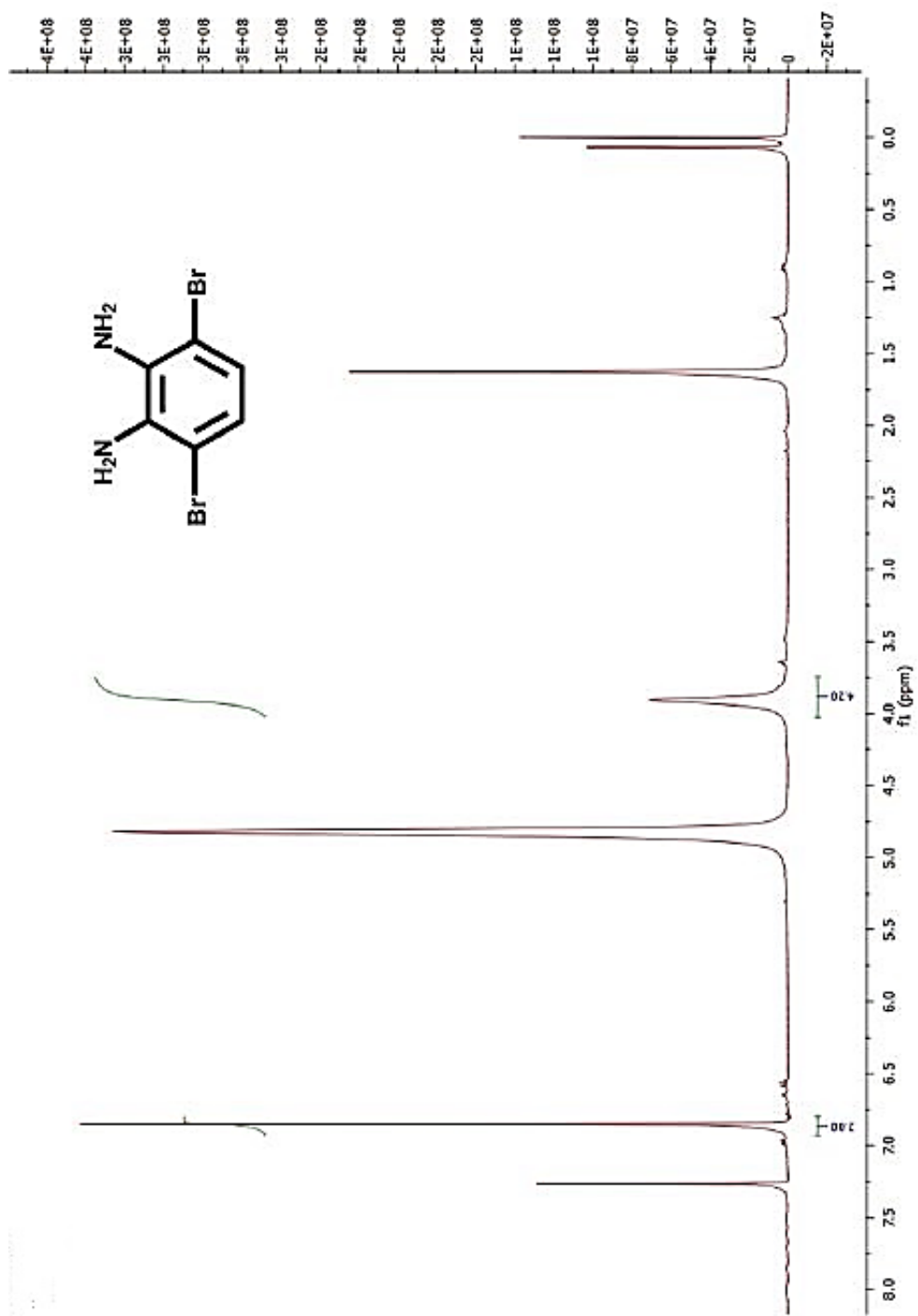


Figure 46. ¹H NMR of 3,6-dibromobenzene-1,2-diamine

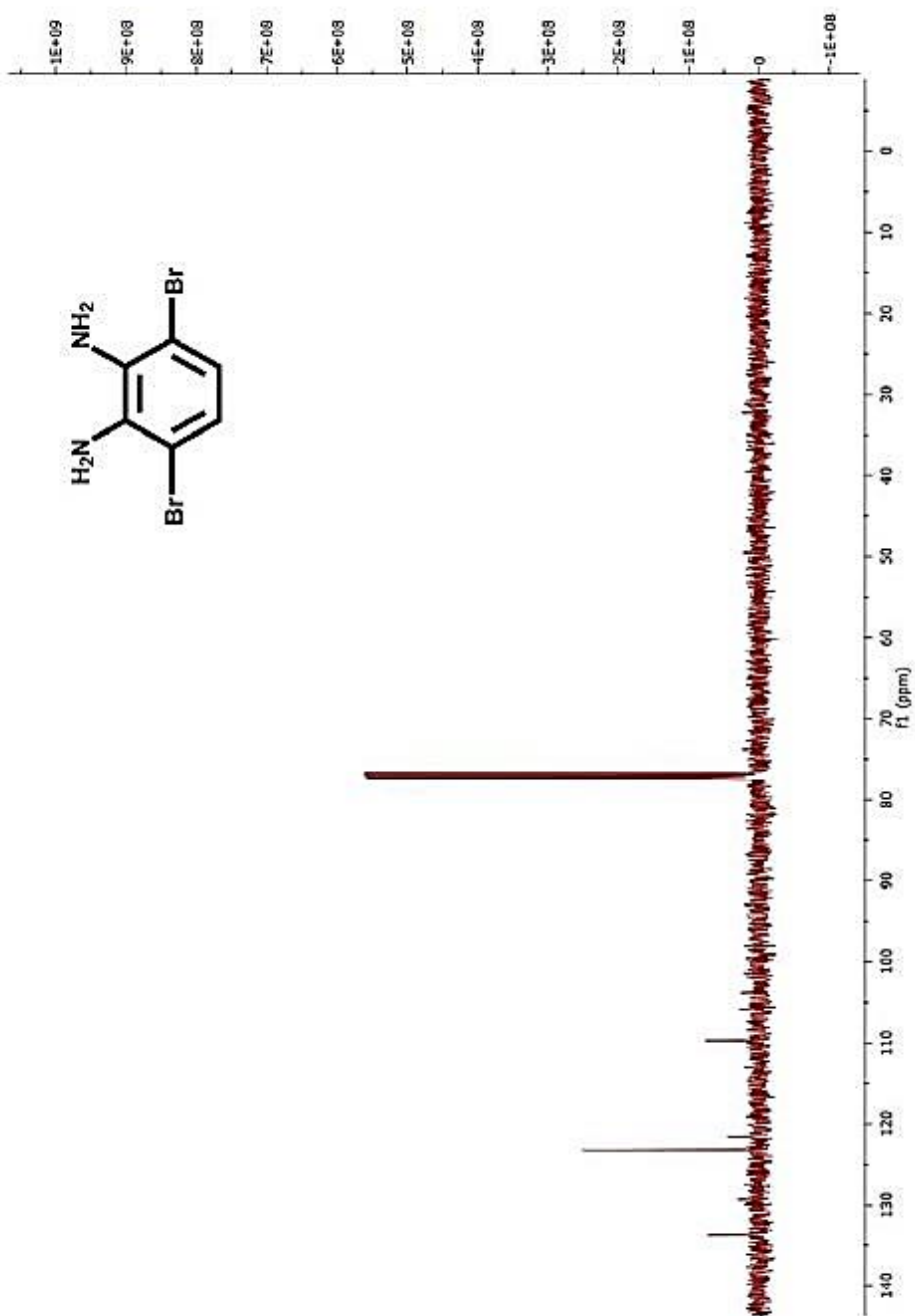


Figure 47. ^{13}C NMR of 3,6-dibromobenzene-1,2-diamine

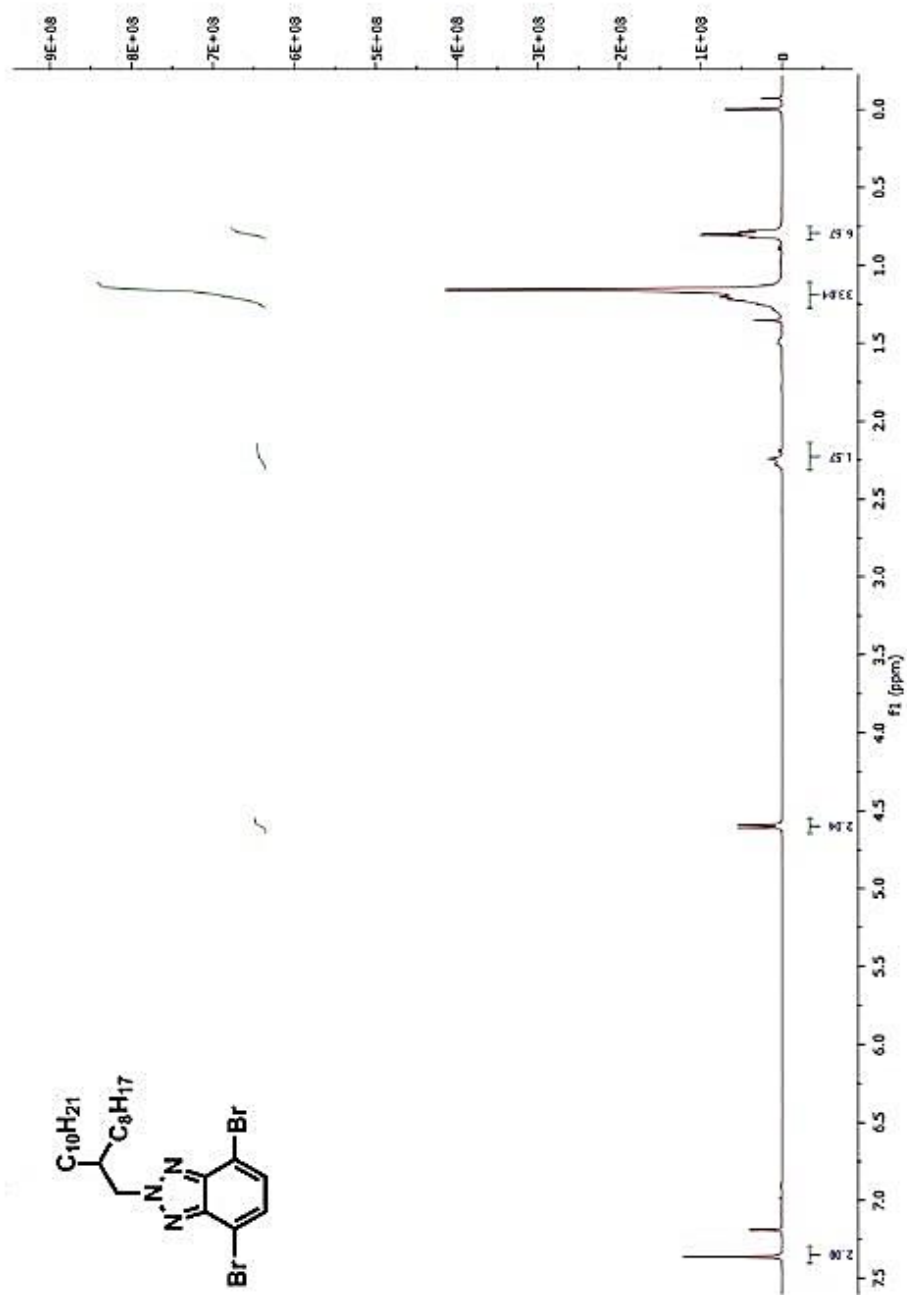


Figure 48. ¹H NMR of 4,7-dibromo-2-(2-octyl-dodecyl)-2H-benzo[d][1,2,3]triazole

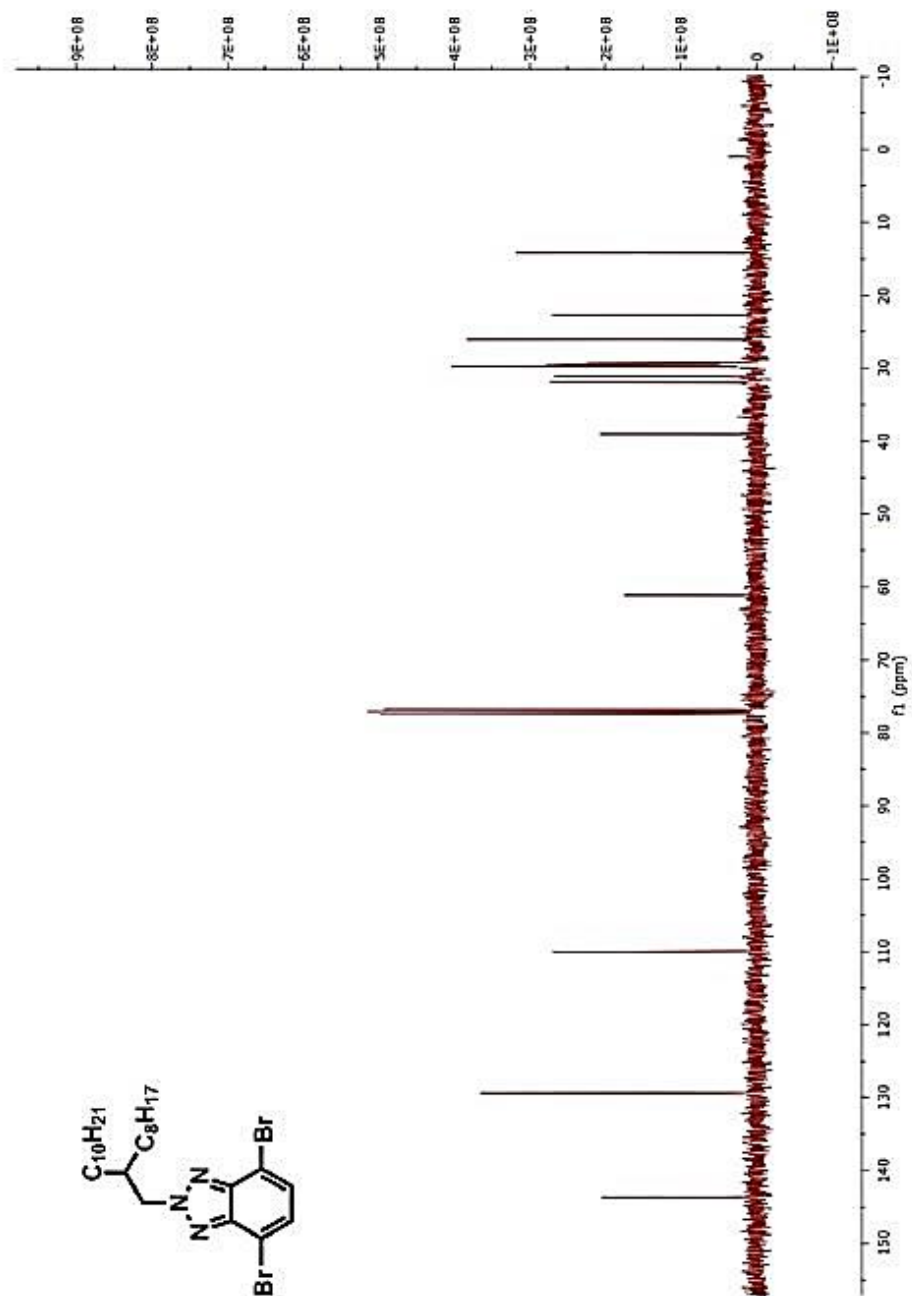


Figure 49. ^{13}C NMR of 4,7-dibromo-2-(2-octyldodecyl)-2H-benzof[d][1,2,3]triazole

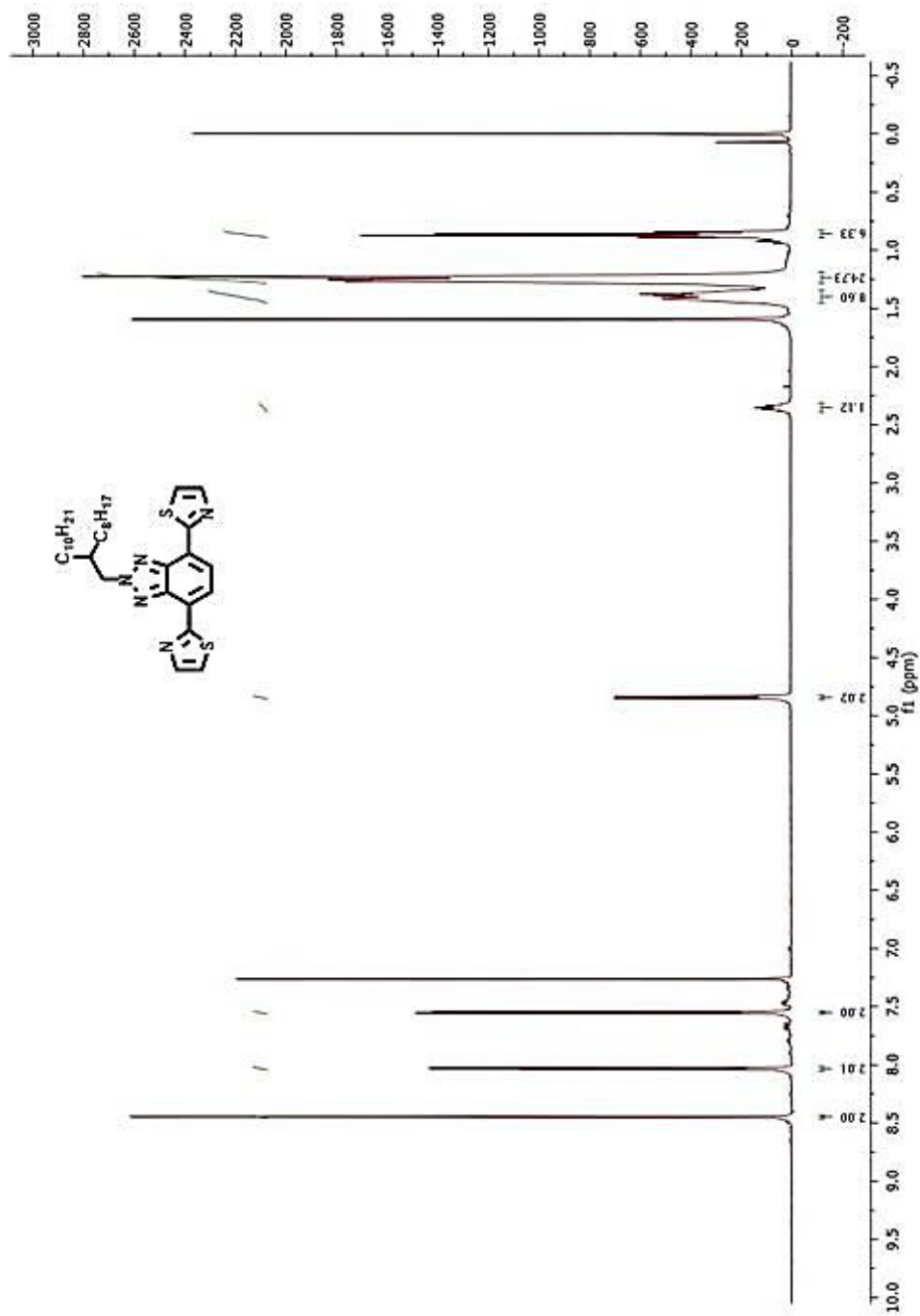


Figure 50. ^1H NMR of 2,2'-(2-(2-octyldodecyl)-2H-benzo[d][1,2,3]triazole-4,7-diyl)dithiazole

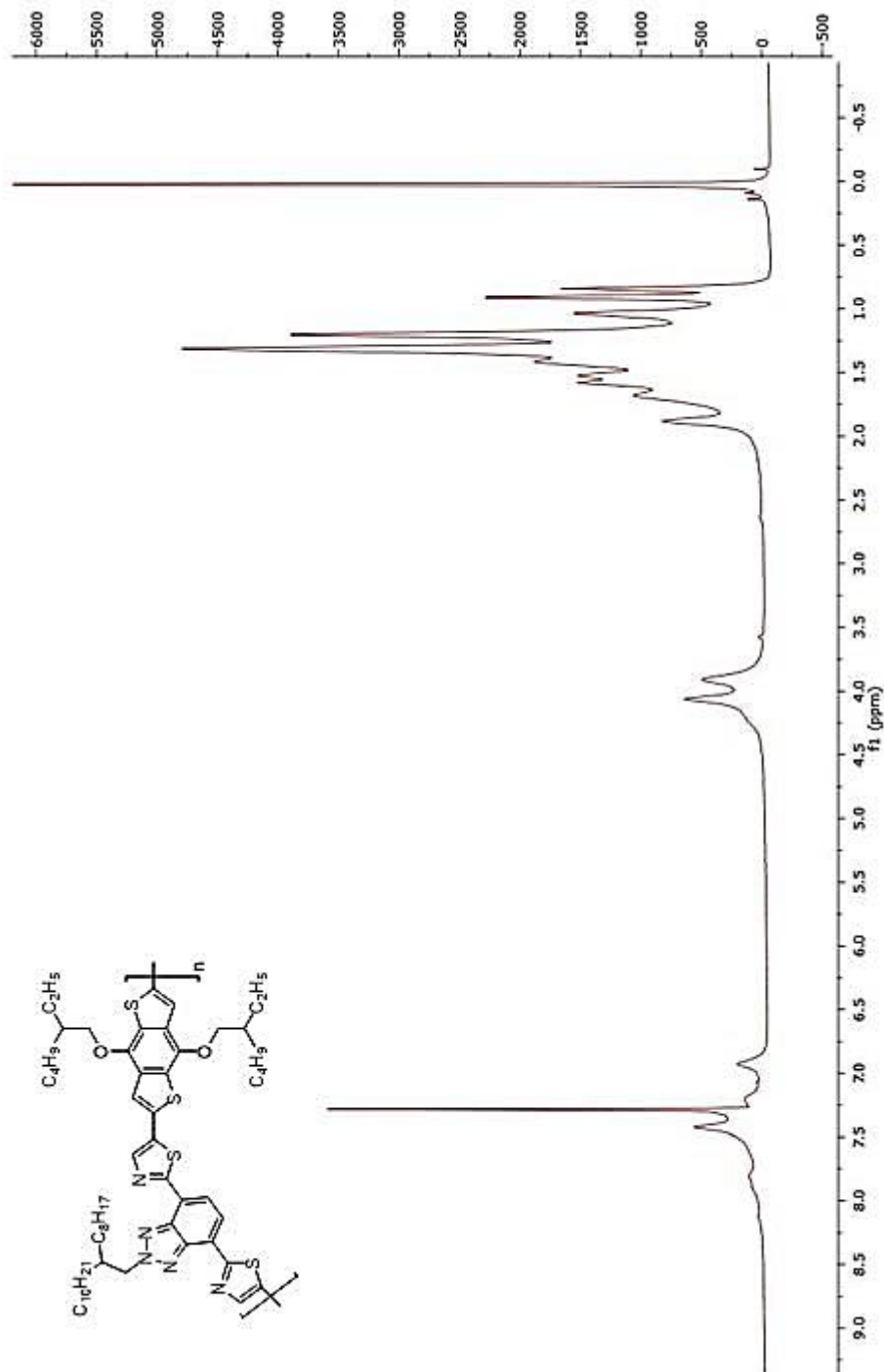


Figure S2. ^1H NMR of P1

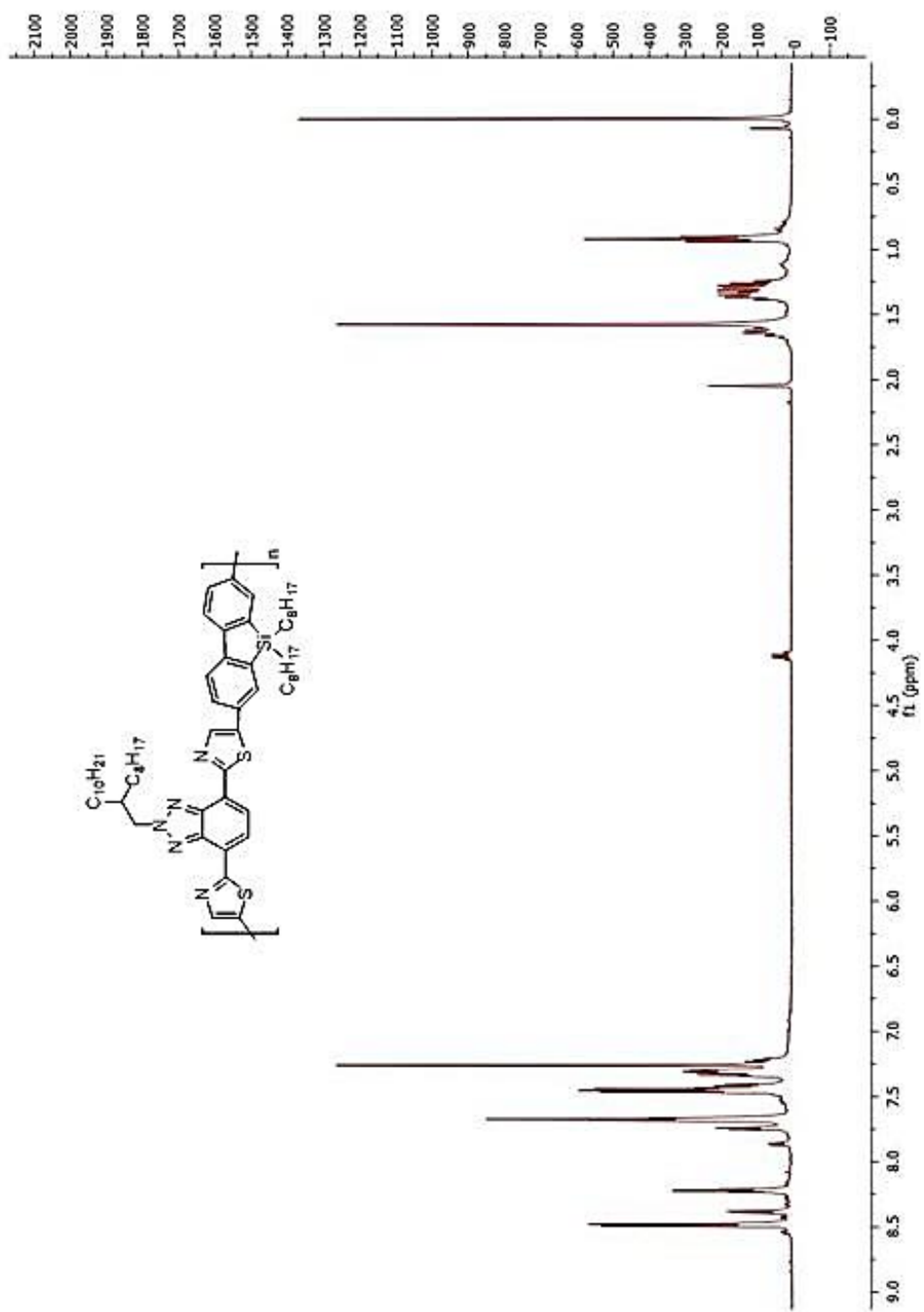


Figure 53. ^1H NMR of P2

THERMAL ANALYSIS RESULTS

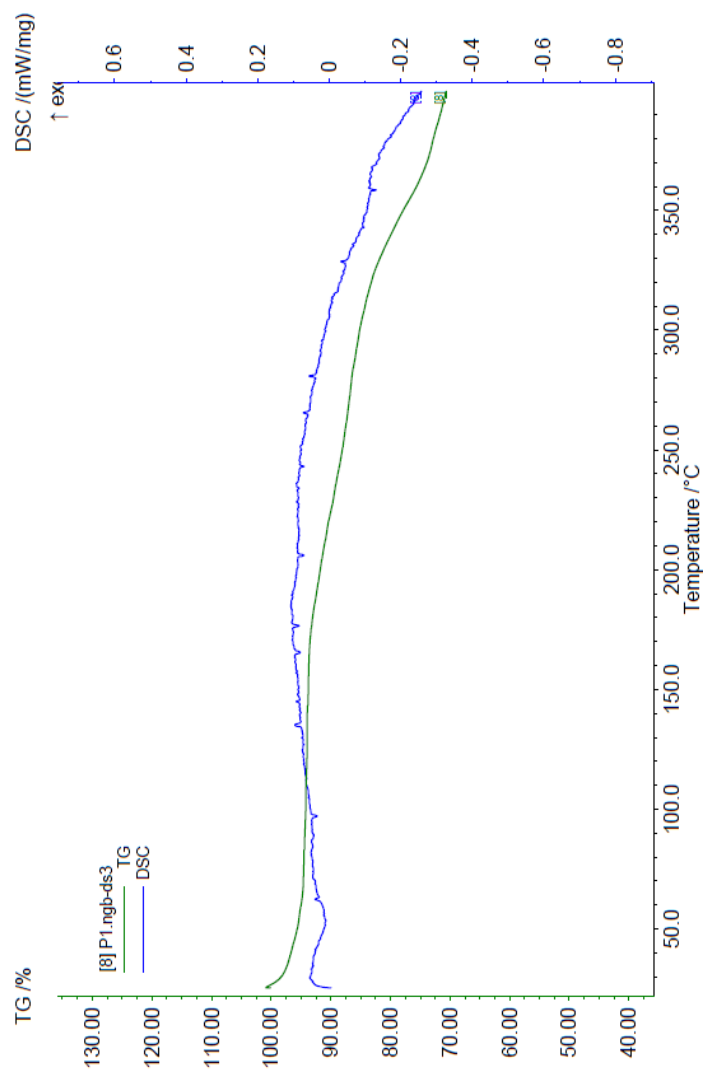


Figure 54. TGA and DSC result of PI

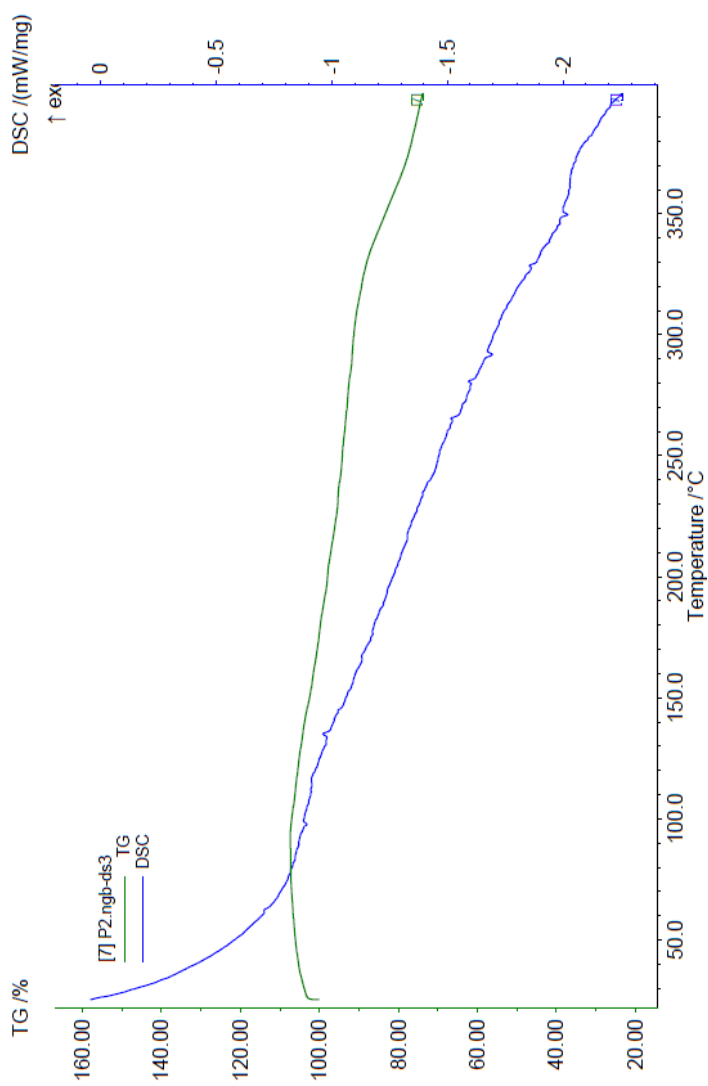


Figure 55. TGA and DSC result of P2